frontiers | Frontiers in Earth Science

TYPE Original Research
PUBLISHED 03 September 2025
DOI 10.3389/feart.2025.1549411

OPEN ACCESS

EDITED BY
Claudia Belviso,
National Research Council (CNR), Italy

REVIEWED BY
Hongjian Zhu,
Yanshan University, China
Sherif Farouk,
Egyptian Petroleum Research Institute, Egypt

*CORRESPONDENCE
Yuhan Huang,
847887578@qq.com

RECEIVED 21 December 2024
ACCEPTED 21 May 2025
PUBLISHED 03 September 2025

CITATION
Huang Y, Wei Y, Wen H, Huo F, Wu X, Guo R, Liao Y, Ruan Y and Jiang H (2025) Study on organic matter depletion in argillaceous limestone of Leikoupo Formation of the Middle Triassic in the central Sichuan Basin: decoupling of organic matter development and preservation conditions under the background of saltwater algae control. *Front. Earth Sci.* 13:1549411.
doi: 10.3389/feart.2025.1549411

Study on organic matter depletion in argillaceous limestone of Leikoupo Formation of the Middle Triassic in the central Sichuan Basin: decoupling of organic matter development and preservation conditions under the background of saltwater algae control

Yuhan Huang[1]*, Yan Wei[1], Huaguo Wen[1], Fei Huo[2], Xueyan Wu[2], Ruiyu Guo[2], Yuntao Liao[1], Yunbo Ruan[1] and Huachuan Jiang[1]

[1]Institute of Sedimentary Geology, Chengdu University of Technology, Chengdu, China, [2]School of Geoscience and Technology, Southwest Petroleum University, Chengdu, China

The Anisian period of the Middle Triassic was a recovery period after the end Permian mass extinction. During this period, a set of organic rich limestone and shale were deposited in the Gypsum lagoon of the Leikoupo Formation in the Sichuan Basin, gradually evolving into a self-generated and self-stored reservoir. This oil and gas reservoir in the 2nd submember of 3rd member of the Middle Triassic Leikoupo Formation ($T_2l_3^2$) was excavated by the CT1 well in the central Sichuan region during recent explorations. However, the previously drilled limestone in Leikoupo Formation in the adjacent PY area has low organic matter abundance and not been able to form a reservoir, and this phenomenon has not been explained yet. To clarify the mechanism of organic matter enrichment in high salinity environments of $T_2l_3^2$ in the PY area, conducting comprehensive analysis using organic and inorganic geochemical techniques. The argillaceous limestone of $T_2l_3^2$ in the PY area is mainly deposited on the edge of the gypsum-limy lagoon, with low *TOC* values ranging from 0.11% to 0.34% and the kerogen of type I-II$_1$. The R_O value ranges from 1.16 to 1.36, with an average of 1.24, indicating that the source rock has reached a high maturity stage. Based on the combination of biomarker compounds and elemental geochemical techniques, it has been found that organic matter mainly comes from planktonic organisms in reducing seawater, accompanied by a small amount of terrestrial organic matter, and the selective enrichment of algae to the environment is also an important factor contributing to differences in organic matter enrichment in local areas.

Furthermore, it can be recognized that the low organic matter abundance in argillaceous limestone in the PY area is controlled by multiple factors. Firstly, dry climate is not conducive to organic matter enrichment. Secondly, the mismatch between productivity conditions and organic matter preservation conditions results in insufficient original organic matter abundance. The decoupling of organic matter development and preservation conditions is the main cause of organic matter depletion in the research subjects. Research on the trend of marine producers towards favorable environments during this period can provide a case study for the enrichment of organic matter in high salinity environments.

KEYWORDS

Earth science, Middle Triassic, limestone reservoir, sedimentary environment, organic geochemistry, organic matter enrichment

1 Introduction

After the extinction at the turn of the Permian and Triassic periods, the recovery of the Earth's marine ecology was relatively slow (Bottjer et al., 2008). During the Middle Triassic, the Leikoupo Formation in the Sichuan Basin was characterized by the widespread development of carbonate platforms, resulting in high salinity. In previous studies, scholars have primarily focused on the development of multiple large-scale dolomite reservoirs in the Leikoupo Formation of Middle Triassic in the Sichuan Basin (Zeng et al., 2007; Wang et al., 2009; Ruan et al., 2022), and the majority believe that the Leikoupo Formation does not develop high-quality hydrocarbon source rocks (Wu et al., 2020; Miao et al., 2022). However, in late 2020, in the Sichuan Basin, Southwest China (Figure 1a), well CT1 for the first time encountered a new type of unconventional reservoir in the 2nd submember of 3rd submember of Lekoupo Formation of Middle Triassic ($T_2l_3^2$), a marine mixed shale reservoir. It is a kind of reservoir with wide distribution, strong hydrocarbon generation ability, large resources, no fault control, nanoscale porosity, micro-fracture development, self-generated and self-storage. Previously, many scholars have proposed that organic rich carbonate rocks can also be authigenic unconventional reservoirs (Katz et al., 2008; Farouk et al., 2022; Farouk et al., 2023), and typically have poor porosity and permeability (Farouk et al., 2024b). The well CT1 of the mixed shale gas reservoir in Leikoupo Formation has obtained industrial gas flow, and the condensate produced has created the highest production record of marine layer condensate in Sichuan Basin, and the exploration potential is huge. This new breakthrough has aroused great concern among researchers.

In recent years, researchers have determined that the mixed shale of $T_2l_3^2$ in central Sichuan Basin is mainly composed of three kinds of shale and part of argillaceous limestone (Sun et al.,2021; Huo et al., 2022; Zhang et al.,2023), among which the argillaceous limestone segment generally exhibits low porosity and low permeability. This kind of mixed shale can be used as source rock or high quality reservoir, and gypsum rock is used as the "cap". However, due to the complex rock fabric, variable mineral combinations, low level of understanding, lack of research materials and other factors of Marine mixed sedimentary shale, especially the first discovery of Marine mixed sedimentary shale in the Leikoupo Formation, Sichuan Basin, there are still few research results on its deposition and formation mechanism.

Prior to well CT, well PY3 in the PY area of central Sichuan also encountered $T_2l_3^2$, which was located at the edge of the Gypsum-limy lagoon facy during the sedimentation period of $T_2l_3^2$ (Wang et al., 2023). As the water becomes shallower, it becomes mainly composed of argillaceous limestone in $T_2l_3^2$ in PY area, which is also mixed with thick layer of gypsum-salt rock, but the abundance of organic matter in the rocks is low, and the industrial oil flow is not generated. The reason for this phenomenon has not been explained.

The key is that this difference directly leads to a lack of reliable basis for predicting future desserts, increasing the risk of predicting favorable areas. Therefore, it is necessary to clarify the organic matter enrichment mechanism and differential genesis of the limestone in order to provide reliable evidence for predicting oil and gas sweet spots. On the other hand, the latest results report on the muddy dolomite as source rock encountered during drilling in a gypsum-salt rock of the 1st member of Leikoupo Formation in central Sichuan Basin, which also suggests that there is a certain influence mechanism on the enrichment of organic matter in high salinity environments (Li et al., 2025). Therefore, the coupling relationship between sedimentary environmental factors such as salinity, productivity, and redox conditions may have a significant impact on explaining differences in hydrocarbon generation capacity.

In order to explain the phenomenon of poor organic matter in the argillaceous limestone of $T_2l_3^2$ near the edge of the gypsum-limy lagoon, based on previous studies, this paper selected the cores and debris of the limestone of Leikoupo Formation in the PY3 well in the central Sichuan Basin. *TOC* values were used to reflect the degree of organic matter enrichment, and biomarkers were used to characterize the degree of algae development. The related factors controlling the development of organic matter were determined by inorganic geochemistry. Through the combination of inorganic and organic geochemistry, this study aims to discuss the causes of organic matter enrichment differences in $T_2l_3^2$, with emphasis on a method to study organic matter enrichment differences in semi-restricted lagoon environments.

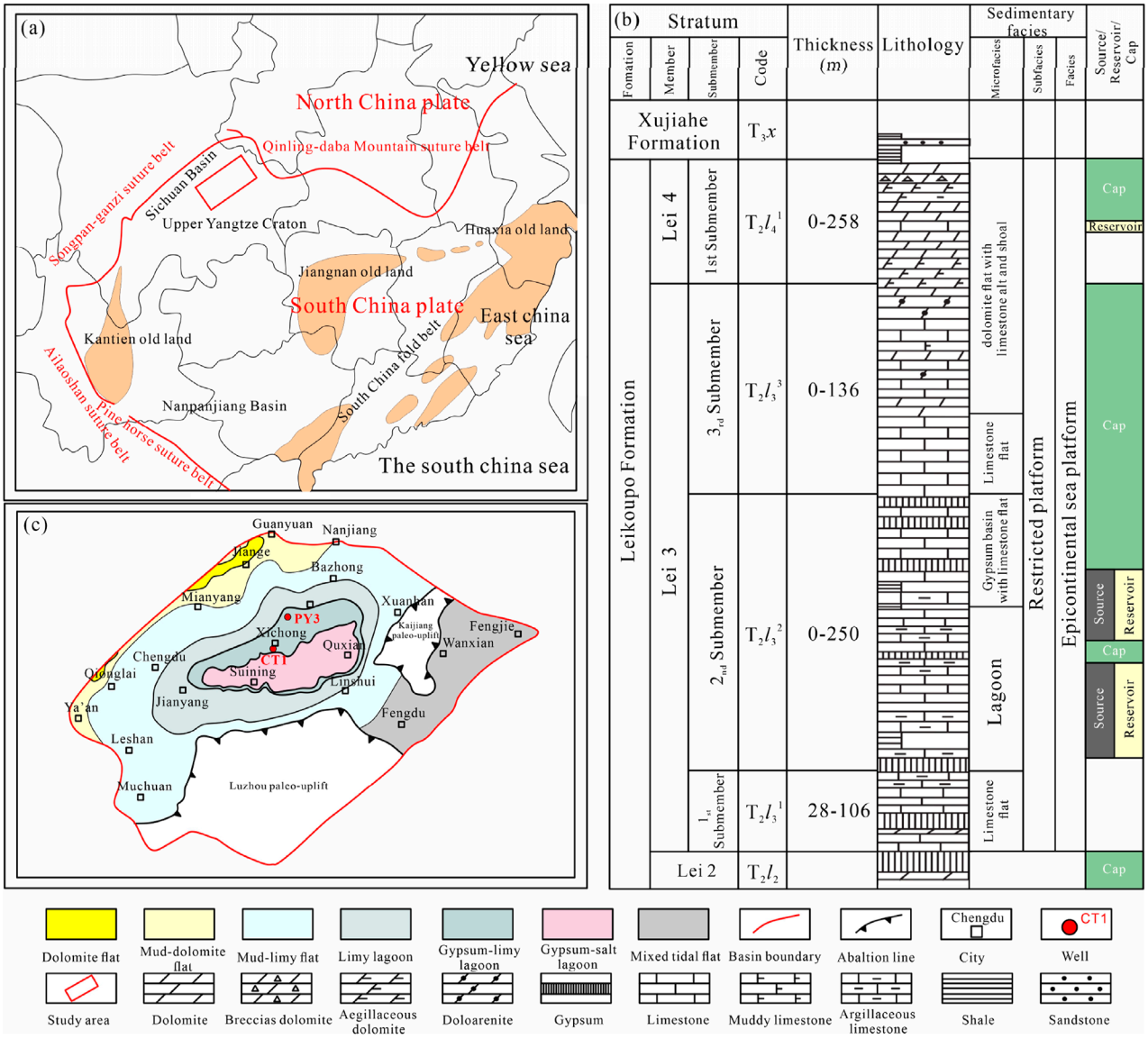

FIGURE 1
The tectonic background and paleogeography of Sichuan Basin **(a)** Paleogeography of South China Plate tectonics during the sedimentation period of Leikoupo Formation; **(b)** Chart of stratigraphy and sedimentary facies of the Leikoupo Formation in the Sichuan Basin (modified from Zhang et al., 2023); **(c)** Sedimentary facies map of the Leikoupo Formation in the Sichuan Basin (modified from Wang et al., 2023).

2 Geological setting

The Sichuan Basin, located in southwest China (Figure 1a), is a typical superimposed basin. The basin is surrounded by a series of mountains, and the interior is dominated by sedimentary rocks, which record the long geological history from the ancient sea to the modern land. The Sichuan Basin has experienced multi-stage and multi-direction deep fault activities since the Indosinian period, forming a rhomboidal tectonic-sedimentary basin, and these activities have led to the characteristics of multi-cycle tectonic and sedimentary evolution of the basin (Feng et al., 1997; He et al., 2011).

The peak period of the Anisian period in the Middle Triassic coincides with the rift action in the Pangaea continent, accelerating the recovery of marine ecosystems. Against this backdrop, the sedimentation of the Leikoupo Formation in the Sichuan Basin was formed. In this global tectonic context, the South China and North China blcoks collided (Figure 1a), and the Mianlue Ocean gradually closed from east to west. The South China block began a strong land-building movement (Chu et al., 2012; Wang et al., 2013), which is characterized by NW trending fold, thrust fault and post-orogenic granite intrusion. The eastward intracontinental subduction of the South China block led to the formation of the Xuefengshan tectonic belt, and the westward compression and migration led to the formation of the Luzhou palaeouplift (Huang et al., 2019; Figure 1c). These tectonic events greatly changed the accumulative environment of the Sichuan Basin (Feng et al., 1997; He et al., 2011).

During the depositional period of the Leikoupo Formation of the Middle Triassic, Sichuan Basin was an assemblage of Paleo-Tethys blocks drifting northward during the Pangaea period (Li et al.,2021). At this stage, a large-scale maritime invasion occurred in the Sichuan Basin, with some seawater entering the Upper Yangtze Basin from the Kaiyuan Strait between the southwestern Kangdian oldland and the northern Vietnam oldland, and then invading the southwestern Sichuan Basin through the Qiannan Barrier Reef. Another part of the seawater enters the basin through the Songpan-Ganzi Trough, through the channel between the Longmen Mountain island chain, or over the underwater seawall (Feng et al.,1997). At the end of the Triassic, the Sibumasu massif collided with the Indian Massif, resulting in the closure of the Ancient Tethys Ocean. Influenced by the early Indosinian movement, the Jiangnan oldland was uplifted sharply, and the topography of Sichuan Basin gradually changed from high in the west to low in the east (Ruan et al., 2022; Zhang et al., 2023). From the perspective of the whole Triassic, Sichuan Basin evolved from Atlantic continental margin in early and Middle Triassic to foreland basin from Late Triassic to Quaternary (Meng et al., 2005; Li et al., 2021). According to the current structural distribution, the Sichuan Basin developed in the northwest of the Upper Yangtze Craton (Figure 1a), thus forming a multi-cycle superimposed oil-gas sedimentary basin (Dai, 1981; He et al., 2017).

The Leikoupo Formation of the Middle Triassic in Sichuan Basin is mainly composed of carbonate and gypsum-salt rocks, which can be divided into T_2l_1, T_2l_2, T_2l_3, and T_2l_4 from the bottom to up (Figure 1b). The T_2l_3 experienced a short period of transgression in the early sedimentary stage, but most of the period was in the regressive state, which can be divided into three submembers: $T_2l_3^1$, $T_2l_3^2$, and $T_2l_3^3$, and the target limestone developed in $T_2l_3^2$.

Controlled by the closure of the eastern segment of the ancient Asian Ocean and the collision between the North China and Mongolian blocks, this subduction collision resulted in the uplift of dolomite flat in the western part of the basin (now around Longmen Mountain), the uplift of Luzhou paleo-uplift in the southern part, and the uplift of Kaijiang paleo-uplift in the eastern part. Thus, a special sedimentary pattern was formed: two uplifted zones sandwiching a low-lying zone. The slopes of Luzhou and Kaijiang palaeouplifts in the central Sichuan Basin are relatively steep, the seawater circulation is limited, and the hydrodynamics are weak. The sedimentary environment is relatively closed and has high salinity, which is mainly manifested in the lagoon environment (Xin et al., 2013; Tan et al., 2014). During the sedimentary period of the $T_2l_3^2$, the Sichuan Basin mainly developed gypsum salt lagoon, gypsum-limy lagoon, limy lagoon, mud-limy flat, mu-dolomite flat, dolomite flat (Figure 1c). The $T_2l_3^2$ in CT1 well which filled with calcareous shale is adjacent to the gypsum-salt lagoon facies. And the PY area, which is developed on the edge of the gypsum-limy lagoon, develops argillaceous limestone (Figure 1c). And as sedimentation progresses, the climate gradually changes from humid to semi humid, and the limitations of water also increase (Huo et al., 2022). Correspondingly at the top, a thick layer of gypsum rock is developed as a good cover layer (Sun et al., 2021) (Figure 1b). Obviously, the lithology of the $T_2l_3^2$ has changed laterally with the position of the sedimentary facies belt.

3 Samples and methods

Carbon isotope geochemistry is directly influenced by major biological fluxes (Maloof et al., 2010). Primary producers prioritize the use of the lighter ^{12}C isotope in their cellular metabolic activities. Therefore, during periods of high primary productivity, the ^{12}C in the water cycle and atmosphere will be depleted, which increases the inorganic ^{13}C content of the carbonate sediments formed during these periods (Brand and Veizer, 1981). In this study, we selected the ^{13}C high-value interval in the Triassic Leikoupo Formation of the PY3 well in the central area of the Sichuan Basin as our research object, which may indicate an active period of producers development (Brand and Veizer, 1981), it is more helpful to understand the controlling factors of organic matter enrichment. Samples were selected at intervals of 0.1 ~ 1.0 m from bottom to up, and the study was carried out based on well logging data. All test analysis mainly includes two parts: organic geochemistry and inorganic geochemistry analysis. The organic geochemical test section includes total organic carbon (*TOC*), kerogen carbon isotope, vitrinite reflectance (R_O), kerogen maceral identification, biomarker analysis. The inorganic geochemical test includes the analysis of major elements and trace elements. Core or rock fragment samples at the same depth are divided into several parts and subjected to the following experiments.

3.1 Organic geochemistry

The instrument used in the *TOC* test is Lectra CS844 carbon and sulfur analyzer, and the standard is GB/T 19,145–2022"Determination of Total organic Carbon in Sedimentary rocks". A total of 21 samples were tested. Firstly, place the porcelain crucible in a muffle furnace and burn it at 900°C ~ 1,000°C for 2 h. After cooling, store it in a dryer. Grind the sample to a particle size of 0.075 mm ~ 0.18 mm, place it in a ceramic crucible, and add hydrochloric acid and distilled water in a 1:7 (volume ratio) hydrochloric acid solution. Heat on a water bath or electric heating plate, with a temperature controlled between 60°C ~ 80°C, and react for more than 2 h until the reaction is complete. Wash the dissolved sample with distilled water until neutral. Place the porcelain crucible containing the sample in an oven at 60°C ~ 80°C for drying, and then test it with an instrument.

The instrument used for the carbon isotope test of kerogen is the MAT 253 stable isotope Mass spectrometer manufactured by ThermoFisher. The experiment adopts the standard SY/T 5238-2019. Firstly, evacuate the sample preparation system to above 2.5 Pa and adjust the oxygen flow rate to 30 mL/min. Introduce the sample preparation system with a carrier gas and set the carrier gas flow rate to 30 mL/min. The temperature of the front furnace of the oxidation furnace rises to 970°C, the temperature of the back furnace rises to 830 C, and the temperature of the silver wire tube section is 400°C–450°C. Connect the carbon dioxide sample collection tube of the sample preparation system, immerse the captured water in anhydrous ethanol cold solution at −80°C ~ −70°C for about 40 mm, and immerse the captured carbon dioxide cold trap in liquid nitrogen for about 40 mm. Subsequently, the sample boat is sent to the high-temperature zone of the front furnace of the sample preparation device, and after gasification, it is carried by the carrier

gas into the oxidation furnace for combustion reaction for 10 min. The carbon dioxide and water generated after the combustion reaction of the sample are captured by the carrier gas in a cold trap for capturing water, and then enter the cold trap for capturing carbon dioxide. Vacuum the cold trap that captures carbon dioxide to above 2.5 Pa, then transfer the carbon dioxide to the sample tube for 5 min. Finally, the sample is sent to an isotope mass spectrometer for analysis.

The reflectance of vitrinite was measured by MSP400 microfluorescence spectrometer based on SY/T 5124-2012. A total of 6 samples were tested. After slicing the rock, pre grind it with sandpaper or corundum powder, and polish it with pool polishing solution. Place the qualified light sheet in the dryer and conduct reflectance measurement after 12 h.

Molecular geochemical analysis was performed on 8 samples. The selection of samples was based on the relatively uniform distribution of the entire source rock. Extraction of about 100 g of sample was successfully obtained by accelerated solvent extraction (ASE) using a Dionex ASE 10 (Thermo Scientific Fischer) and 40 mL dichloromethane as extractant. The extraction was carried out at 100°C and 100 bar for 15 min. After the extract was evaporated, the residue was dissolved in n-pentane. Then sodium sulphate (Na_2SO_4) and active copper powder were added to remove the excess water and sulphur. Continuously, the extracted organic compounds were divided into 3 fractions on column chromatography, by using different polarity eluents: 6 mL pentane to get aliphatic fraction, 6 mL pentane to get aromatic fraction, 6 mL methanol to get NSO fraction. Composition analysis of aliphatic and aromatic fractions was performed using gas chromatography (GC-FID) and gas chromatography mass spectrometry (GC-MS). The analysis of aliphatic fractions was carried out by GC-FID using Fisons Instruments GC 8000 with a Zebron ZB-1 fused silica column (internal diameter: 0.25 mm, film thickness: 0.25 μm). Hydrogen was used as the carrier gas in the experiment. The temperature was initially set at 70°C for 3 min, then heated at a rate of 5°C per minute, and finally maintained at 310°C for 20 min. The aliphatic and aromatic hydrocarbons were analysed by GC-MS with HRGC 5160 (Mega series) gas chromatography, Zebron ZB-5, coupled with fused silica column (internal diameter: 0.25 mm, film thickness: 0.25 μm) and connected to a quadrupole mass spectrometer (Thermoquest). In the single-ion monitoring (Sim) mode, the MS analysis worked in the electron impact ionization (EI) mode at 70 eV, and helium was used as the carrier gas. The temperature was initially set at 70°C for 3 min, heated to 160°C at a rate of 10°C·min^{-1}, then heated from 160°C to 320°C at a rate of 3°C per minute, and finally maintained at 320°C for 20 min. The aromatic fraction was heated at an initial temperature of 70°C for 3 min, then at a heating rate of 3°C per minute to 320°C, maintained at that temperature for 20 min. Peak identification was based on published data. Xcalibur software was used for peak area integration.

The instrument used for the identification of kerogen macerals was Axio Imager. M 2 m fluorescence microscope, and the detection was based on SY/T 5125-2014. After obtaining the kerogen macerals, it is necessary to calculate the TI index to classify the kerogen types. The formula used is:

$$TI = (A \times 100 + B \times 50 - C \times 75 - D \times 100)/100) \quad (1)$$

In Formula 1, A represents percentage content of sapropelic group; B represents the percentage of chitin; C represents the percentage of vitrinite; D is the percentage of inertinite.

3.2 Element geochemistry

A total of 26 samples were used for major and trace element analysis. Firstly, pour 2–3 g of the sample into an envelope and place it in an open oven at 105 C Celsius for 2 h. After drying, take out each sample from the oven and place it in a glass dryer. Weigh about 0.30 g of lithium metaborate in a graphite crucible, then weigh about 0.05 g of sample, mix evenly, and place the graphite crucible into a ceramic crucible. Put it into a muffle furnace and set the temperature to 860°C for melting. Pour into a plastic bottle containing 30 mL of 5% concentrated dilute nitric acid, place it on a shaker, shake for about 2 h until the molten salt is completely dissolved. Dilute Milli-Q pure water to 100 mL. After the sample preparation is completed, ICP-AES with the model number Thermo ICAP 7000 is used for testing.

Prior to the experiments, powdered shale samples (200 mesh) were calcined in a high-temperature furnace (700 C) to completely remove organic matter. Before the experiments, shale samples were placed into a polytetrafluoroethylene (PTFE) vessel with a mixed solution of $HClO_4$, HF and HNO_3 to dissolve powdered samples. After the sample preparation is completed, ICP-MS with the model number Agilent 7,900 is used for testing and analysis.

After obtaining the oxide Al_2O_3 content, the element content should be calculated using the formula as follows:

$$X_{Element} = M_{Element}/M_{Oxides} \times \omega_{Oxides} \times 10^4 \quad (2)$$

In Formula 2, $X_{Element}$ represents the element content in the sample (μg/g); $M_{Element}$ represents the molar mass of the element (g/mol); M_{Oxides} represents the molar mass (g/mol) of the corresponding oxide of the element. ω_{Oxides} represent the mass percentage (%) of the element corresponding to the oxide in the sample.

Aluminum is mainly derived from aluminosilicate clay (Murray, 1994; Sageman et al., 2003). Titanium is commonly associated with clay and heavy minerals, including ilmenite and rutile (Calvert and Pedersen, 1993). Thus, Al and Ti concentrations are used to assess the contribution of local terrigenous sources in modern and ancient Marine systems (Tribovillard et al., 2006). Before the use of trace element test data, Al or Ti elements are usually used to correct trace elements, which is used to calculate non-debris or excess elements, and obtain the corresponding excess value, so as to eliminate the interference of terrestrial materials. The standard values of elements in Australian Post-Archean shales (PAAS) were used for standardization, and the standard values were derived from Nance and Taylor (1976). In this study, Al is adopted as the correction element, and the correction formula used is as follows:

$$X_{XS} = X_{sample} - Al_{total} \times (X/Al)_{PAAS} \quad (3)$$

In Formula 3, X_{XS} is the content of elements from non-clastic sources in the sample; X_{sample} is the total content of the element in the sample. Al_{total} is the content of Al element in the sample. The $(X/Al)_{PASS}$ is the ratio of this element to Al in the Post-Archean Australian Shales (PAAS).

Chemical alteration index (CIA) is often used to indicate the chemical weathering intensity of clastic rocks (Nesbitt and Young, 1982), and is often used in clastic rock studies to determine paleoenvironment, climate change, and sediment sources. Higher CIA values generally indicate strong weathering and humid climate conditions, while lower CIA values may reflect weak weathering or dry climate conditions. In the diagenetic process, due to the influence of potassium metasomatism, the CIA index is usually offset, which needs to be corrected by using the correction formula (Panahi et al., 2000), which is publicized as follows:

$$CIA = \text{mole}\left[Al_2O_3/\left(Al_2O_3 + CaO^* + Na_2O + K_2O\right)\right] \times 100 \quad (4)$$

For the calculation and correction of CaO, the formula is adopted:

$$CaO^* = \text{mole}\,CaO - \text{mole}P_2O_5 \times 10/3 \quad (5)$$

In Formulas 4, 5, molar fraction is used for each element, and CaO^* represents the molar fraction of CaO in silicates. The author used the method proposed by McLennan (1993) to correct CaO^*: If the corrected mole of CaO is less than the mole of Na_2O, the corrected mole of CaO is used as the mole of CaO. In contrast, the mole number of Na_2O is used as the mole number of CaO.

The contents of Fe, Mn, Cr, V, Ni and Co in sedimentary rocks are higher in humid climate. Under dry conditions, due to the evaporation of water and the enhancement of alkalinity, Ca, Mg, K, Na, Sr, Ba are precipitated to form a large number of salts deposited at the bottom, so their content is relatively high. Using the ratio of these two elements, the climate index C can be calculated as follows:

$$C = \sum(Fe + Mn + Cr + V + Ni + Co)/(Ca + Mg + K + Na + Sr + Ba) \quad (6)$$

In Formula 6, the unit of content of all elements is μg/g.

The sediment contains detrital particles from different sources and with different properties that will impact the analysis results. Therefore, it is necessary to eliminate the influence of detrital particles (Tang et al., 2015). The priority is transforming Mo and U concentrations into the EF_X form, using the following equation:

$$X_{EF} = (X/Al)_{sample}/(X/Al)_{PAAS} \quad (7)$$

In Formula 7, X indicates a certain element. The $(X/Al)_{sample}$ is the ratio of this element to Al in the sample. The $(X/Al)_{PASS}$ is the ratio of this element to Al in the Post-Archean Australian Shales (PAAS).

4 Result

4.1 Organic geochemistry

4.1.1 Organic compound characteristics

The *TOC* values of samples of argillaceous limestone in the PY3 well range from 0.11% to 0.34%, with an average of 0.21. The R_O value ranges from 1.16 to 1.36, with an average value of 1.24. The carbon isotope values of kerogen range from−30.1‰ to −28.2‰, with an average of − 29.425‰. In the microscopic components of kerogen, all samples are mainly composed of sapropelinite (60% ~ 73%), appearing orange or brownish orange, with dispersed shapes; Next is the exinite (24% ~ 36%), which retains the residual appearance of native plants. The calculated TI index ranges from 72 to 83.75, with an average value of 78.25.

4.1.2 Biomarker compounds

In the saturated hydrocarbon chromatography results of PY3 well, nC_{17} and nC_{18} can be identified by using Pr and Ph. The main peak carbon of n-alkanes is concentrated in nC_{18}~nC_{20}, and the Pr/Ph ratio ranges from 0.22 to 0.57, with an average value of 0.32. The $C_{21} + C_{22}/C_{28} + C_{29}$ values range from 14.75 to 26.37, with an average value of 19.87.

4.2 Element geochemistry

4.2.1 Trace element

The results of trace element testing are shown in Table 1. After calculating the excess value of elements using the Al content in PAAS standard, we create a box plot of the distribution of some key geochemical indicators, which can provide a more intuitive understanding of the patterns(Figure 2).The V/Cr ratio of the argillaceous limestone in the Leikoupo Formation ranges from 0.017 to 10.575, with an average value of 2.068; The V/(V + Ni) ratio ranges from 0.074 to 0.853, with an average value of 0.500; The U/Th ratio ranges from 2.585 to 59.400, with an average of 17.774 (Figure 2).

4.2.2 Major element

The test results of major elements are shown in Table 2. The content of Al_2O_3 is 0.094–7.526, with an average of 2.307. After calculation, the content of Al element is 58.68–1242.06 μg/g, with an average of 417.58 μg/g. The content of CaO ranges from 23.7 to 52.2, with an average of 42.410. The content of Na_2O ranges from 0.043 to 0.495, with an average of 0.223. The content of K_2O ranges from 0.026 to 2.186, with an average of 0.609. The content of P_2O_5 ranges from 0.003 to 0.062, with an average of 0.024; The TiO_2 content ranges from 0.012 to 0.254, with an average of 0.085.

Using element testing data for calculation (Figure 2), the CIA index was found to be between 31.126 and 71.661, with an average value of 60.193; The C index ranges from 0.001 to 0.054, with an average of 0.018; The ancient productivity index Ni/Al ranges from 0.0004 to 0.0068, with an average value of 0.0017, and P/Al ranges from 0.0023 to 0.1099, with an average value of 0.2355; The paleosalinity index Ca/(Ca + Fe) ranges from 0.9400 to 0.9991, with an average value of 0.9801.

In well PY3, the salinity growth boundary was preliminarily identified based on the development positions of dolomite and gypsum salt rock, and divided into three parts: I, II, and III (Figure 2). From the boxplot (Figure 2), the distribution of values of TOC, CIA, C index, V/Cr, V/(V + Ni), and U/Th in the limestone in Part I is higher than that in Parts II and III. The distribution of values of Ca/(Ca + Fe), P/Al, Ni/Al in the limestone in Part I is lower than that in Parts II and III.

10.3389/feart.2025.1549411

TABLE 1 Data of trace element of argillaceous limestone in $T_2l_3^2$ in Sichuan basin.

Samples			V	Cr	Co	Ni	Mo	Th	U
ID	Well	Depth(m)	μg/g	μg/g	μg/g	μg/g	μg/g	μg/g	μg/g
1	PY3	4,065.0	9.43	4.81	1.05	4.86	0.44	0.61	2.03
2	PY3	4,066.0	2.30	2.06	0.090	2.07	2.35	0.18	0.35
3	PY3	4,070.0	2.69	5.64	0.10	3.47	0.17	0.13	0.58
4	PY3	4,071.0	22.4	11.8	1.36	5.91	2.72	0.96	2.70
5	PY3	4,072.0	4.54	2.96	0.22	2.56	0.53	0.32	1.76
6	PY3	4,073.0	2.16	66.9	0.14	4.59	0.26	0.13	0.71
7	PY3	4,074.0	12.4	3.65	0.82	5.88	0.54	0.46	1.55
8	PY3	4,075.0	3.10	3.69	0.046	2.32	0.23	0.19	0.74
9	PY3	4,077.2	3.67	2.84	0.11	3.28	0.90	0.17	0.58
10	PY3	4,079.9	1.10	5.62	0.084	3.75	0.23	0.097	0.11
11	PY3	4,080.6	1.77	3.22	0.059	2.10	0.091	0.11	0.11
12	PY3	4,081.1	26.5	13.8	3.10	8.45	1.55	2.61	2.76
13	PY3	4,082	36.3	26.0	5.24	12.7	1.79	3.96	3.50
14	PY3	4,082.2	57.8	38.6	9.05	19.9	1.48	5.77	4.42
15	PY3	4,082.5	54.1	38.5	8.04	18.1	1.65	5.39	4.31
16	PY3	4,082.8	45.9	28.3	6.60	17.1	1.88	4.30	4.52
17	PY3	4,083.3	49.2	30.7	6.50	15.4	1.94	4.90	5.97
18	PY3	4,084.2	19.7	12.1	2.55	8.70	0.82	1.84	4.12
19	PY3	4,084.7	13.7	9.14	1.70	7.33	0.33	1.09	2.94
20	PY3	4,085	37.8	26.3	4.95	13.4	1.26	3.08	4.89
21	PY3	4,085.3	44.4	87.6	6.23	37.5	1.94	3.63	5.69
22	PY3	4,085.8	10.9	6.70	1.33	5.18	0.32	0.53	2.16
23	PY3	4,086	13.4	9.78	1.79	6.17	0.34	0.61	2.45
24	PY3	4,086.3	69.4	54.7	9.72	28.0	3.61	6.59	8.57
25	PY3	4,086.7	20.3	9.86	1.60	6.31	0.60	0.78	3.37
26	PY3	4,087	22.7	11.9	1.86	6.62	0.71	0.97	4.59

5 Discussion

5.1 Petrology characteristics

Under the microscope, it was observed that the main mineral composition of the argillaceous limestone in $T_2l_3^2$ in the PY area is micritic calcite (Figure 3a), containing some clay (Figure 3a), and some samples contain a small amount of gypsum (Figure 3b). Scanning electron microscopy shows that the interior of the argillaceous limestone mainly develops intergranular pores of calcite and clay (Figure 3c,d), as well as shrinkage joints formed by clay dehydration (Figure 3d), and there are also few organic matter pores (Figure 3d).

There are significant differences in the properties between the argillaceous limestone of lagoon facies of $T_2l_3^2$ and common dolomite reservoirs. The dolomite reservoir is significant due to its high

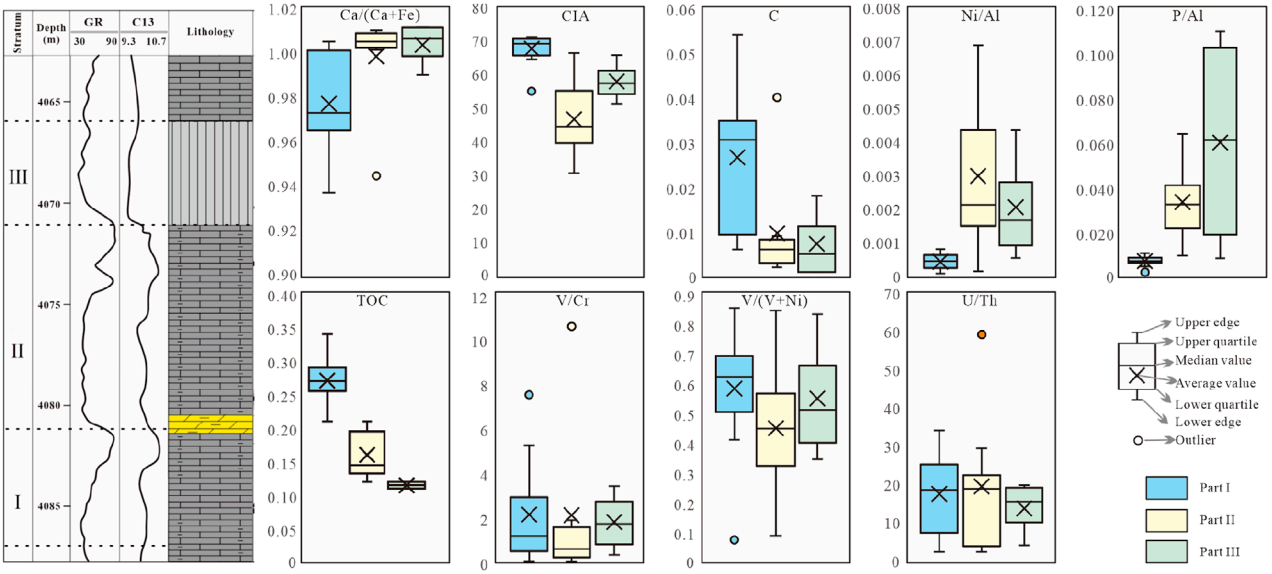

FIGURE 2
Box plot of geochemical indicators of argillaceous limestone of $T_2l_3^2$ in PY3 well.

porosity and permeability, which is attributed to the pore increasing effect formed by the dolomitization of its original limestone and various fluid dissolution processes (Wen et al., 2021). In contrast, the argillaceous limestone of $T_2l_3^2$ exhibits characteristics of low porosity and low permeability, mainly composed of pore structures formed by primitive sedimentary minerals as the main storage space, and does not have microscopic features of foreign fluid dissolution. The enrichment of clay or organic matter enhances the plasticity of rocks, making pores more susceptible to compaction effects. Some clay are partially compacted due to the lack of protection from rigid minerals, but another portion of clay intergranular pores are still preserved. Due to the production of natural gas from kerogen after hydrocarbon generation, the gas expansion rate during the process can exceed 50% (Ungerer, 1990). Therefore, the maintenance of pore morphology may be related to the high-pressure gas support generated by hydrocarbon generation in a closed environment, and the abnormal ultra-high pressure generated is the key to pore preservation. For example, The pressure coefficient of $T_2l_3^2$ of CT1 well reaches 1.96, which may be related to hydrocarbon-generating pressurizatio.

5.2 Organic matter characteristics

TOC value is an evaluation index of organic matter abundance, which can be used for evaluating source rocks and reflecting marine productivity during sedimentary periods (Makky et al., 2014; Huo et al., 2022; Qteishat et al., 2024). The total organic carbon (*TOC*) content of argillaceous limestone in $T_2l_3^2$ ranges from 0.11% to 0.34%, with an average value of 0.21. The organic matter abundance exceeds the minimum threshold for hydrocarbon generation in carbonate rocks, indicating that argillaceous limestone in $T_2l_3^2$ has a certain ability to generate hydrocarbons. But the quality is obviously not as good as the shale in CT1 (with an average *TOC* value of 0.88%; Zhang et al., 2023). The R_O value of vitrinite reflectance in source rocks ranges from 1.16 to 1.36, with an average of 1.24, indicating that the source rocks have basically reached a high maturity stage.

However, in terms of logging interpretation, this interval does not have oil and gas indications. The maturation of hydrocarbons is the reason that affects the residual abundance of organic matter, especially when rocks tend towards higher maturity. Under higher maturity conditions, hydrocarbon generation is mainly dominated by the production of pyrolysis gas (Figure 4; Nie et al., 2022), and a large amount of hydrocarbons are broken down into gas and detached from rocks, resulting in the loss of original organic matter in rocks. However, previous records have shown that the argillaceous limestone and calcareous shale of $T_2l_3^2$ in CT1 well have higher R_O, and their residual *TOC* values are still higher than argillaceous limestone of $T_2l_3^2$ in PY3 well. This indicates that the ability of argillaceous limestone in PY area of Sichuan Basin to enrich primitive organic matter is indeed inferior to that in CT area. Therefore, we tend to consider its low abundance of original organic matter.

After researching multiple oil and gas rich basins in China, previous researchers have summarized a suitable classification scheme for kerogen in the Sichuan Basin: Type I kerogen has a $\delta^{13}C$ value between −35‰ and −30‰, Type II_1 kerogen has a $\delta^{13}C$ value between −30‰ and −27.5‰, and Type II_2 kerogen has a $\delta^{13}C$ value between −27.5‰ and −25‰; The $\delta^{13}C$ value of type III kerogen is greater than −25‰ (Huang, 1998). The carbon isotopes of kerogen in the argillaceous limestone of $T_2l_3^2$ range from −30.1‰ to −28.2‰, with an average value of −29.425‰. All samples are mainly composed of sapropelinite (60%~73%), presenting a brownish orange color with dispersed shapes; Next is the exinite (24% ~ 36%), which retains the residual appearance of native plants (Figures 3e, f). In addition, the sample also contains a very small amount of vitrinite. When the TI index is greater than 80, it indicates type I kerogen, and 40–80 indicates type II_1 kerogen (Cao, 1985). The TI index of kerogen in $T_2l_3^2$ marine argillaceous limestone ranges from 72 to 83.75, with an average of 78.25. Based on

10.3389/feart.2025.1549411

TABLE 2 Data of major element of argillaceous limestone in $T_2l_3^2$ in Sichuan basin.

Samples			SiO_2	TFe_2O_3	Al_2O_3	CaO	K_2O	MgO	Na_2O	TiO_2	P_2O_5	MnO	LOI
ID	Well	Depth (m)	%	%	%	%	%	%	%	%	%	%	%
1	PY3	4,065.0	2.122	0.47	0.59	50.000	0.11	1.519	0.14	0.033	0.016	0.009	39.400
2	PY3	4,066.0	0.16	0.048	0.14	42.700	0.026	0.25	0.043	0.017	0.017	0.002	7.175
3	PY3	4,070.0	0.14	0.038	0.14	42.800	0.030	0.28	0.048	0.017	0.018	0.002	8.457
4	PY3	4,071.0	3.184	0.88	1.066	47.100	0.24	2.750	0.15	0.051	0.011	0.009	29.700
5	PY3	4,072.0	0.72	0.14	0.35	48.600	0.095	1.192	0.094	0.021	0.010	0.004	26.000
6	PY3	4,073.0	0.15	0.11	0.13	43.100	0.060	0.31	0.059	0.014	0.008	0.002	8.237
7	PY3	4,074.0	1.125	0.38	0.49	39.400	0.16	4.732	0.10	0.027	0.011	0.005	11.900
8	PY3	4,075.0	0.29	0.35	0.20	41.600	0.058	4.558	0.092	0.016	0.007	0.004	11.000
9	PY3	4,077.2	0.30	0.29	0.21	46.500	0.083	4.260	0.086	0.019	0.010	0.005	9.472
10	PY3	4,079.9	0.011	0.25	0.096	42.000	0.032	0.61	0.074	0.012	0.004	0.002	2.766
11	PY3	4,080.6	0.074	0.10	0.094	44.100	0.046	0.88	0.081	0.015	0.007	0.003	3.102
12	PY3	4,081.1	10.200	1.726	2.462	29.400	0.63	14.400	0.29	0.11	0.029	0.015	36.400
13	PY3	4,082	15.100	1.481	4.946	36.600	1.346	6.011	0.50	0.17	0.053	0.019	32.900
14	PY3	4,082.2	21.600	2.075	7.526	31.800	2.186	3.592	0.43	0.25	0.060	0.023	29.900
15	PY3	4,082.5	20.500	2.001	6.999	32.600	1.933	4.078	0.47	0.24	0.062	0.022	30.000
16	PY3	4,082.8	16.200	1.524	5.429	38.300	1.351	2.682	0.40	0.19	0.054	0.020	33.200
17	PY3	4,083.3	15.500	1.456	5.469	38.800	1.363	2.231	0.45	0.21	0.054	0.018	32.900
18	PY3	4,084.2	6.022	0.67	2.189	48.300	0.48	1.386	0.26	0.076	0.024	0.012	39.800
19	PY3	4,084.7	3.841	0.51	1.448	50.500	0.29	1.199	0.19	0.052	0.019	0.011	41.500
20	PY3	4,085	14.100	1.231	4.823	40.500	1.340	2.179	0.30	0.15	0.039	0.016	34.700
21	PY3	4,085.3	15.100	1.419	5.368	39.600	1.483	2.009	0.35	0.17	0.047	0.016	33.700
22	PY3	4,085.8	2.327	0.43	0.93	52.200	0.20	0.74	0.15	0.031	0.011	0.008	42.500
23	PY3	4,086	3.341	0.33	1.018	51.448	0.40	0.57	0.21	0.014	0.003	0.005	42.200
24	PY3	4,086.3	12.400	1.333	4.624	23.700	1.192	1.531	0.33	0.22	0.027	0.014	35.212
25	PY3	4,086.7	4.248	0.38	1.501	50.600	0.33	0.66	0.23	0.043	0.012	0.006	41.400
26	PY3	4,087	4.619	0.48	1.753	50.400	0.38	0.64	0.27	0.052	0.012	0.007	40.800

the comprehensive analysis of carbon isotopes and microscopic components of kerogen, it is determined that the kerogen type of the Leikoupo Formation argillaceous limestone is I-II_1 type sapropelic humic amorphous form.

When the R_O values of type I and II kerogen are between 1.16 and 1.36, the source rock is in the peak period of pyrolysis gas production and the formation of organic matter pores (Figure 4; Yang, 2017; Nie et al., 2022). The low porosity and low permeability of the argillaceous limestone have to some extent promoted the *in-situ* retention of oil and gas. Natural gas cannot migrate through effective transport channels and is stored in poorly connected pores, leading to the formation of ultra-high pressure mentioned above. Therefore, argillaceous limestone of $T_2l_3^2$ has a certain self-generation and self-storage capacity, and its tight characteristics are conducive to the formation of pore overpressure, thus enabling it to have the ability to preserve pores.

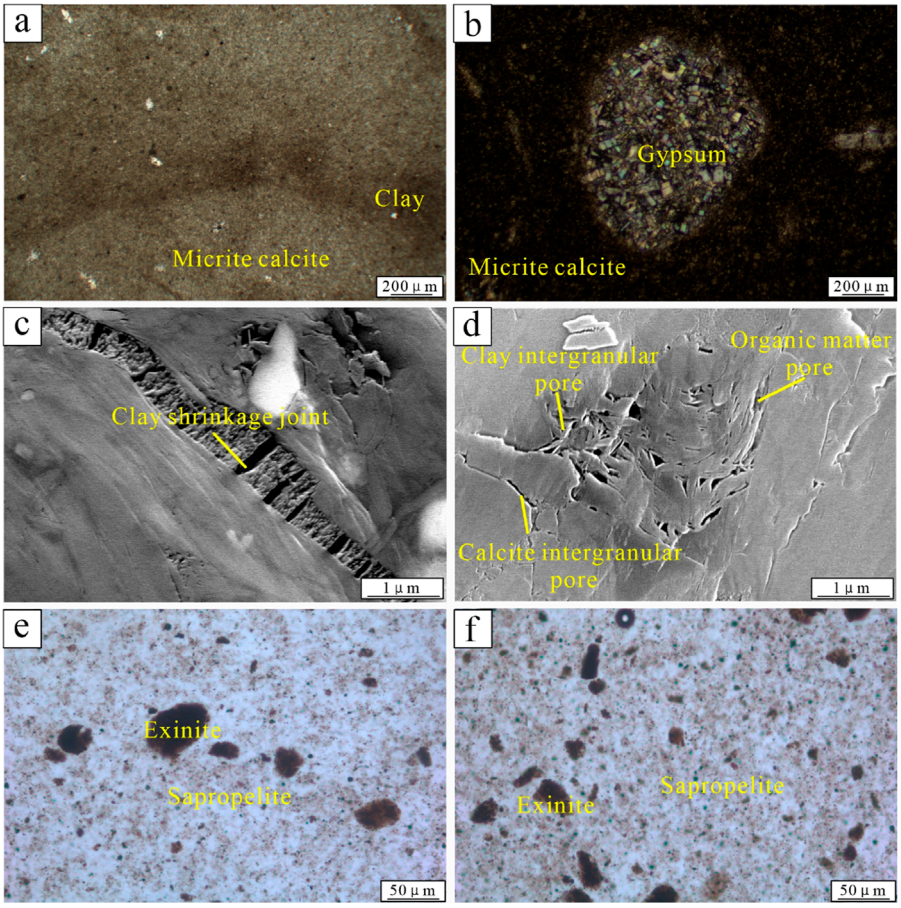

FIGURE 3
Micrographs of argillaceous limestone of $T_2l_3^2$ in PY3 well. **(a)** Micrite calcite, PY3 well, 4,082.4 m, single polarization; **(b)** Micrite calcite and gypsum, PY3 well, depth 4,080.6 m, orthogonal polarization; **(c)** Clay shrinkage joints in the mud laminae, PY3 well, 4,082.4 m; **(d)** Intergranular pores of calcite and clay, a small amount of organic matter pores, PY3 well, 4,080.6 m; **(e)** Sapropelinite with exinite, PY3 well, 4,082.4 m; **(f)** Sapropelinite with exinite, PY3 well, 4,080.6 m.

However, compared to the argillaceous limestone and shale interbedded in the CT1 well near the center of the lagoon (Figure 1c), the hydrocarbon generation capacity of this argillaceous limestone is clearly weaker. The *TOC* values of $T_2l_3^2$ argillaceous limestone and shale in CT1 well ranges from 0.11% to 4.00%, with an average of 0.88% (Zhang et al., 2023), and the organic matter abundance is much higher than that in PY area.

5.3 Source of organic matter

The use of biomarker compound technology can trace the source of organic matter and preliminarily identify sedimentary environmental characteristics (Marynowski et al., 2000; Zeman Kuhnert et al., 2023). The test results of vitrinite reflectance (R_O) of argillaceous limestone in $T_2l_3^2$ indicate that the rock has not reached the overmature stage, and the degree of organic matter cracking is not high. The UCM peak appears gentle, indicating a low degree of bitumen cracking (Figure 5). The use of biomarker compounds to invert sedimentary environments is still reliable.

The main peak carbon of n-alkanes of argillaceous limestone in the PY3 well is concentrated around nC_{18}, with a low carbon number advantage, reflecting the similarity in organic matter sources between the two, mainly from primitive bacteria or algae in the lagoon (He et al., 2016; Sahoo et al., 2020). The ratio of Pr/nC_{17} and Ph/nC_{18} in PY3 and CT1 wells was used for sampling (Zhang et al., 2023), and the results showed that the organic matter in all $T_2l_3^2$ samples mainly came from planktonic algae in the reducing environment, while a small amount of organic matter belonged to mixed organic matter, that is, mixed with terrestrial organic matter(Figure 6; Qteishat et al., 2024). Therefore, the organic matter of the argillaceous limestone in the Leikoupo Formation is mainly derived from marine sources, mixed with a very small amount of terrestrial organic matter.

5.4 Environment of organic matter enrichment

The GR curve and C13 curve exhibit characteristics of slow rise and rapid decline, indicating the presence of multiple cycles of slow

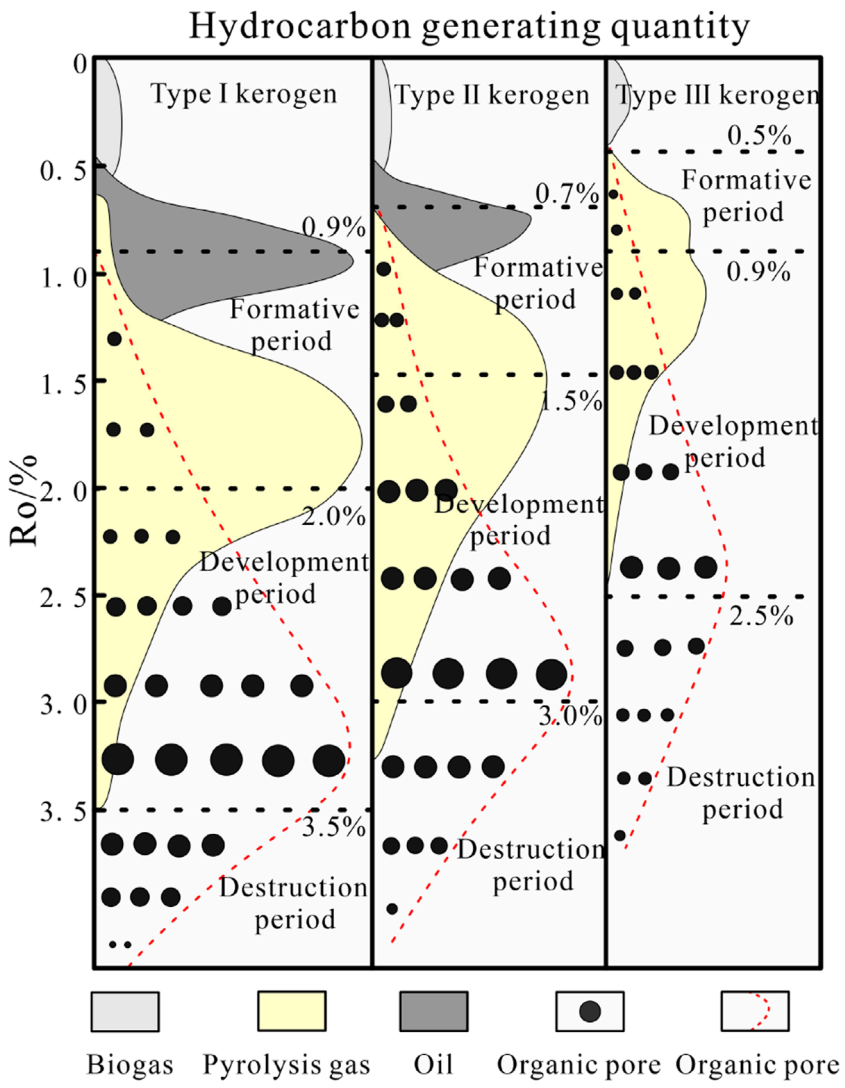

FIGURE 4
Development and evolution of organic matter pores (according to Yang, 2017; Nie et al., 2022).

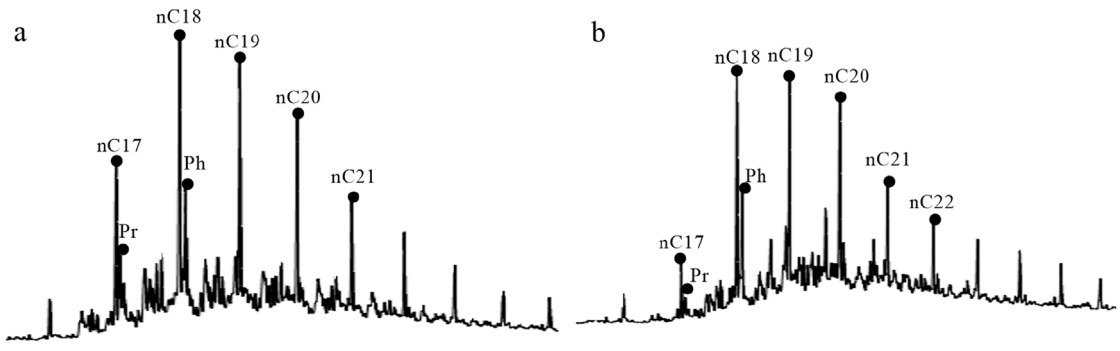

FIGURE 5
Distribution map of n-alkanes of argillaceous limestone in $T_2l_3^2$. **(a)** PY3 well, 4,081.2 m; **(b)** CT1 well, 4,077.4 m.

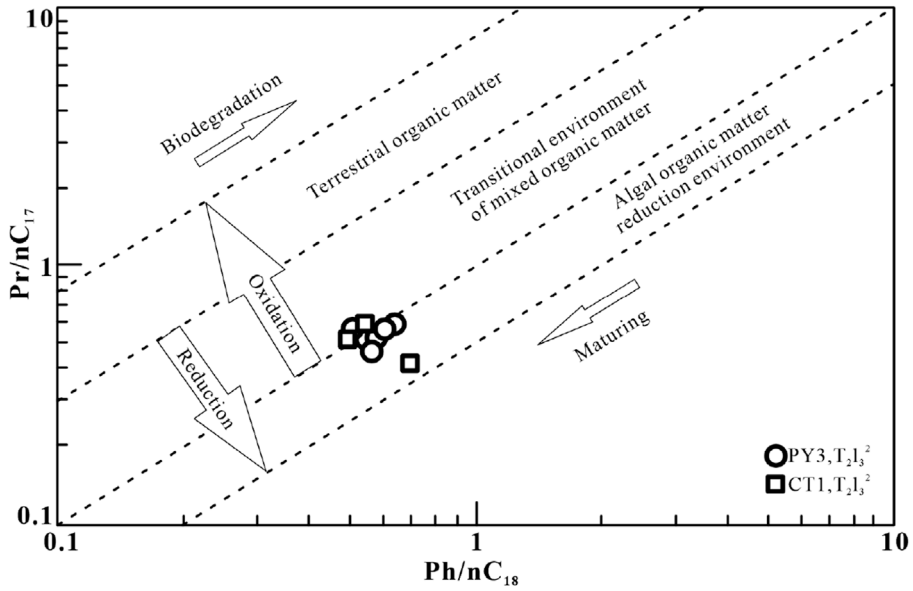

FIGURE 6
Ratio of Pr/nC_{17} and Ph/nC_{18} of source rock in $T_2I_3^2$. (The data of CT1 well comes from Zhang et al., 2023).

and rapid regression during the sedimentary period. Changes in sea level can affect sedimentary environments, which in turn can impact the development and composition of organisms (Farouk et al., 2024a). The appearance of the upper gypsum salt rock highlights the overall trend of regression. Based on the appearance of dolomite and thick layer gypsum salt at the top, we divided the study interval in the PY well into three parts: I, II, and III (Figure 7). The sudden appearance of dolomite and gypsum salt rock from bottom to top reflects the rapid changes in the environment during this period, which may indicate a rapid increase in salinity and a rapid drying of the climate as a whole, as shown in relevant indicators (Figure 7). And the comparative study of this rapidly changing environmental stage in different drilling wells is conducive to highlighting the differences in organic matter enrichment ability in different regions during the same period of environmental changes. In terms of sedimentary environment research, the alteration of fine-grained sedimentary rocks by late diagenesis is weak, and they contain the most complete Earth's historical records (Aplin and Macquaker, 2011). Therefore, researchers usually use their characteristics to restore their sedimentary environment features (Floyd et al., 1990; Huo et al., 2022). Biological activities and pyrolysis can degrade organic matter, resulting in complex structures of hydrocarbons that are difficult to separate, leading to the formation of bulging UCM peaks in chromatography (Xiao et al., 2022). The weak correlation between R_O and *TOC* (R^2 = 0.0183; Figure 8a), as well as the flat characteristics of the UCM peak in saturated gas chromatography (Figure 5), indicate the reliability of using organic geochemical indicators for inversion. The distribution characteristics and ratio changes of major trace elements in sedimentary rocks are important geochemical indicators for reconstructing ancient sedimentary environments. By combining organic geochemistry with inorganic geochemistry techniques, the reliability of research data is ensured.

5.4.1 Terrestrial input

Zr is usually used as a coarse particle input indicator (Chen et al., 2003), while Al_2O_3 is usually used as a fine particle input indicator (Canfield, 1994). Through correlation analysis of terrestrial input indicators Al_2O_3, TiO_2, Zr and *TOC*, it was found that there is a certain positive correlation between organic matter enrichment and terrestrial input with low content, indicating that terrestrial input has some impact on organic matter enrichment. Due to the characteristics of biomarker compounds indicating that organic matter is mainly derived from marine plankton, and the degree of terrestrial input is relatively low, it is believed that the main contribution of terrestrial input to organic matter enrichment should be reflected in the input of nutrients, rather than the large amount of terrestrial organic matter carried. Moderate terrestrial input may carry abundant nutrients into the water, promote biological growth, and enrich organic matter, but excessive terrestrial input has a significant dilution effect on organic matter (Figures 7C,D, 8b). From a vertical perspective, during the sedimentation process in the lower part of the selected well section, there was a sudden decrease in terrestrial input. Due to the overall low abundance of organic matter, the decline in organic matter was not as severe as indicators such as terrestrial input (Figure 7).

5.4.2 Paleoclimate, paleosalinity, and paleoproductivity

Chemical weathering is closely related to paleoclimate and is an effective method for tracking climate change (Fedo et al., 1995; Nesbitt and Young, 1982). The CIA index shows a positive correlation with Al and *TOC* values (Figures 8e,f), especially with strong coupling with terrestrial input indicators. Therefore, it is inferred that strong chemical weathering produces more debris, which can input more nutrients into the ocean and promote the production of organic matter. According to the classification criteria,

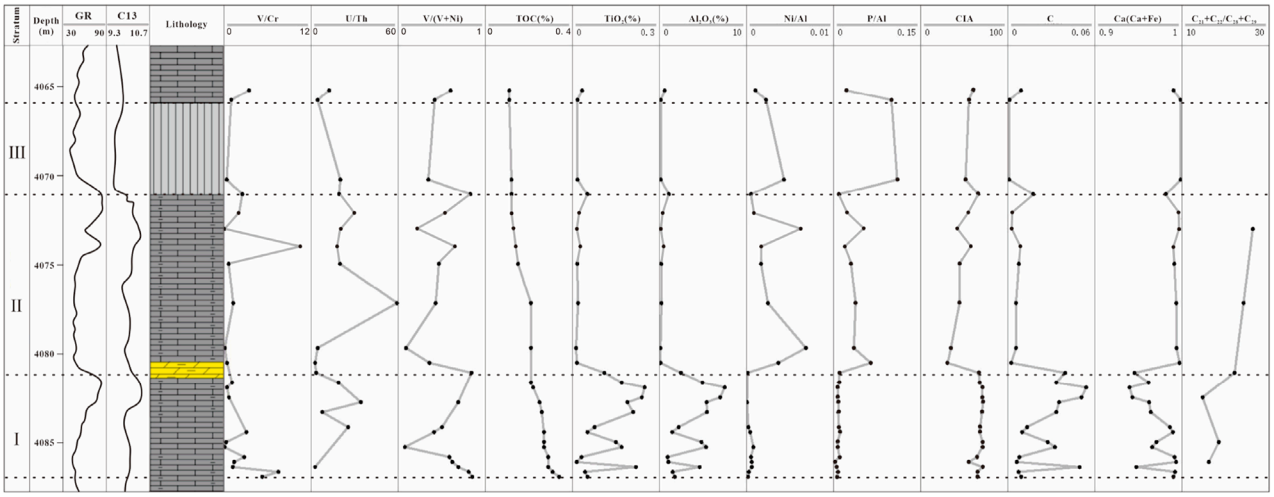

FIGURE 7
Longitudinal changes of redox, terrigenous input, paleoproductivity, CIA, C index, paleosalinity, and *TOC* in PY3 well.

a C index between 0-0.2 indicates a dry climate, 0.2–0.4 indicates a semi dry climate, 0.4–0.6 indicates a semi dry to semi humid climate, 0.6–0.8 indicates a semi humid climate, and greater than 0.8 indicates a humid climate (Qiu et al., 2015). The C index of the samples is concentrated between 0.001 and 0.054 (Table 2), all falling within the dry climate range. Therefore, the climate during the argillaceous limestone sedimentation period in the study section was relatively dry, and the chemical weathering intensity represented by the CIA index is clearly strongly coupled with the climate conditions represented by the C index (Figure 8). Vertically, the climate during the sedimentation period became increasingly dry, leading to an increase in water salinity, which is consistent with the trend of changes in the paleosalinity index Ca/(Ca + Fe), especially at the junction of Parts I and II, where paleosalinity and paleoproductivity rapidly increased simultaneously (Figure 8).

In addition, we found that salinity, productivity indicators, and *TOC* are decoupled (Figure 8g,i), but salinity indicators are coupled with paleoproductivity indicators (Figure 8j). This phenomenon may indicate that seawater salinity has an impact on productivity, but due to other factors, organic matter was ultimately not preserved in large quantities. In saturated hydrocarbon chromatography, the C_{21} + C_{22}/C_{28} + C_{29} values reflect the degree of enrichment of lipid rich compounds such as algae in the hydrocarbon parent material, which can indicate the source of organic matter and sedimentary environment (Philippi, 1974). In this study, we consider it as an indicator of the proportion of algae development. The experimental results indicate that the C_{21} + C_{22}/C_{28} + C_{29} values are well correlated with paleosalinity indicators Ca/(Ca + Fe), paleoproductivity indicators P/Al, Ni/Al, etc. (Figure 8k,m). Vertically, the C_{21} + C_{22}/C_{28} + C_{29} values also increased with the increase of paleoproductivity and paleosalinity, indicating a significant increase in the development of phytoplankton (Figure 7). This indicates that planktonic algae, as the main source of organic matter, are to some extent dependent on salinity, and the increase in salinity promotes the development of algae and facilitates primary production processes. Even closer to the top of the gypsum salt section, there was a further increase in ancient productivity. In Sections 1, 2, planktonic algae, paleosalinity, and paleoproductivity remained positively coupled without decoupling, which may indicate that the salinity changes in seawater remained within a suitable range for algal development. The above phenomenon indicates that suitable water salinization can to some extent stimulate primary productivity such as planktonic algae. The third section of gypsum salt rock lacks asphalt and there are no suitable samples for biomarker compound testing, but the presence of gypsum salt indicates that the salinity of seawater is also very high.

The terrestrial input also suggests the influence of salinity on algae. In the higher stage of terrestrial input (I) accompanied by low salinity, it indicates the possibility of mineral dilution by terrestrial freshwater input. Under the potential influence of freshwater input, the values of C_{21} + C_{22}/C_{28} + C_{29} are relatively low, indicating that freshwater input is not suitable for algal development.

Halotolerant microorganisms maintain cell osmotic pressure balance under high salinity conditions through partial osmotic adaptation strategies such as intracellular small molecule compatible solute accumulation, but their biological activity is relatively low. Halophile microorganisms exhibit good activity under high salt conditions due to their high osmotic adaptation strategies such as salt solubility (Chen et al., 2022). However, this study suggests that in high salinity environments (where dolomitization occurs and salinity indicators are high), algal lipid synthesis is enhanced (C_{21} + C_{22}/C_{28} + C_{29} values increase), suggesting that high salinity environments stimulate the activity of related algae, thereby suggesting that the main response to environmental changes may be halophilic algae. However, halophilic algae can only develop rapidly within a relatively narrow range of salinity and are highly sensitive to changes in salinity (Uratani et al., 2014; Wang, 2018).

Furthermore, we have to raise a question: during the process of regression, the shallowing of water is more conducive to the development of primary producers, but why did the changes in

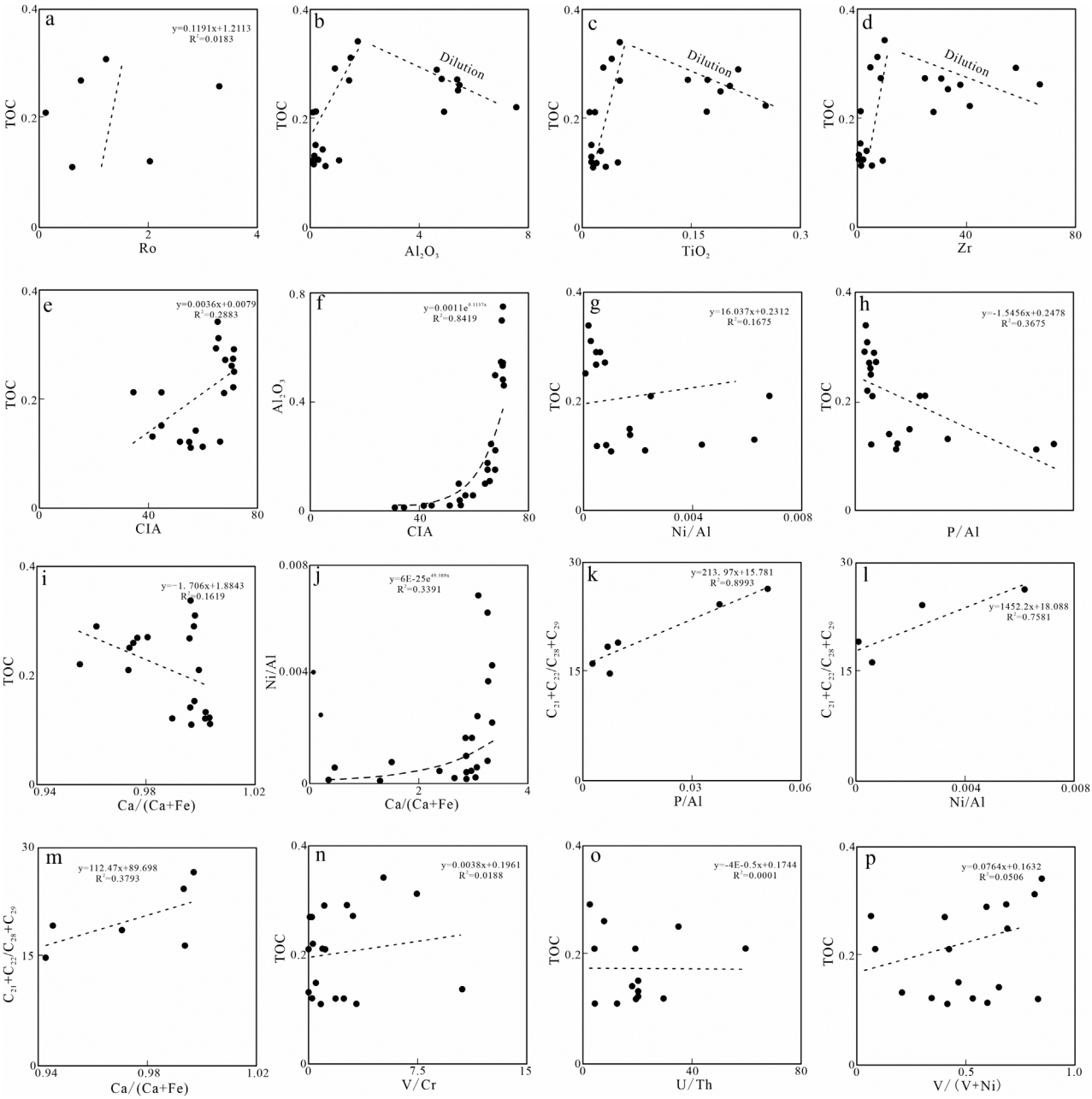

FIGURE 8
(a) Correlation plot between TOC and RO; **(b)** Correlation plot between TOC and Al2O3; **(c)** Correlation plot between TOC and TiO2; **(d)** Correlation plot between TOC and Zr; **(e)** Correlation plot between TOC and CIA; **(f)** Correlation plot between Al2O3 and CIA; **(g)** Correlation plot between TOC and Ni/Al; **(h)** Correlation plot between TOC and P/Al; **(i)** Correlation plot between TOC and (Ca/Ca+Fe); **(j)** Correlation plot between Ni/Al and (Ca/Ca+Fe); **(k)** Correlation plot between C21+C22/C28+C29 and P/Al; **(l)** Correlation plot between C21+C22/C28+C29 and Ni/Al; **(m)** Correlation plot between C21+C22/C28+C29 and Ca/(Ca+Fe); **(n)** Correlation plot between TOC and V/Cr; **(o)** Correlation plot between TOC and U/Th; **(p)** Correlation plot between TOC and V/(V+Ni).

paleoproductivity, paleosalinity, and *TOC* values not show a strong positive correlation? We have to shift our focus to the preservation conditions of organic matter.

5.4.3 Redox condition

Considering that the synergistic increase in paleoproductivity and paleosalinity did not respond to changes in *TOC* values, it is necessary to consider the preservation conditions of organic matter. It is generally believed that the degree of oxidation-reduction in the sedimentary environment of source rocks is crucial for the preservation of their organic matter. A single oxidation-reduction indicator is not reliable and requires a comprehensive analysis using different indicators. We also need to acknowledge that there are slight differences between the restorative indicators, so we cautiously use them to analyze trends rather than conducting high-precision quantification.

When the ratio of Pr and Ph is less than 1, it usually indicates a reducing environment, which is consistent with the ratio of Pr and Ph in argillaceous limestone. In addition, it is generally believed that the significant advantage of Tm content indicates a reducing environment, while the significant advantage of Ts content indicates an oxidizing environment. The Ts/Tm ratio in the sample ranges from 0.66 to 0.77, indicating an advantage in Tm content and indicating a relatively reduced seawater environment.

When V/Cr is between 2 and 4.25, it indicates a suboxic environment. The V/Cr ratio in the sample ranges from 0.017 to 10.575, with an average of 2.068, which is generally consistent with the suboxic environment (Ernst, 1970). When both V and Ni are enriched, it indicates that they are in a sulfide rich environment, but V is more sensitive than Ni. Therefore, changes in the V/(V + Ni) ratio in sediments can be used to indicate relative changes in oxygen (Hatch and Leventhal, 1992). When the sediment V/(V + Ni) is between 0.45 and 0.60, it indicates a suboxic environment; When it is between 0.54 and 0.82, it indicates a sulfur free reducing environment. The V/(V + Ni) ratio in argillaceous limestone ranges from 0.074 to 0.853, with an average value of 0.500, indicating a suboxic environment as a whole. U is prone to precipitate in a tetravalent state in a reducing environment. Therefore, the U/Th ratio can reflect the redox conditions of sedimentary water and is a commonly used measurement parameter for the redox conditions of sedimentary environment (Adams and Weaver, 1958; Ahmad et al., 2019). Many corrected Th elements exhibit negative values, which may have been heavily influenced by diagenesis and resulted in losses, The U/Th ratio may be too high, so the reference value of this indicator is poor.

There are certain differences between organic and inorganic materials. Considering the impact of terrestrial inputs on biomarkers, we believe that the overall environment is more inclined towards a suboxic environment. And the water environment is actually constantly fluctuating between oxidation and reduction (Figure 7).

The GR curve to some extent reflects changes in sea level height. The V/Cr, U/Th, and V/(V + Ni) ratios match well with the GR curve, demonstrating the correlation between redox conditions and sea level changes, indicating that the trend indicated by the indicators is reliable. The overall performance of Section 1 is characterized by a more realistic approach. The reducibility of the dolomite section at the bottom of Section 2 sharply decreased (Figure 7), even showing suboxic conditions, but the reducibility increased in its upper part. When entering the third stage of the development of the large set of gypsum salt rocks, the sea level rapidly drops and enters the oxidation stage again. The positions of the two GR negative deviations correspond to the appearance of dolomite and gypsum salt rocks, as well as a sudden decrease in reducibility. Overall, the reducibility of water in Sections 2, 3 is not good, and the conditions for organic matter preservation are unfavorable, which is consistent with the trend of *TOC* value changes.

5.4.4 Limitation of seawater

In order to understand the synergy between external seawater supply and salinity, this paper discusses the limitations of the water environment in sedimentary areas. Identification through Mo-TOC and Mo_{EF}-U_{EF} covariant model (Algeo and Lyons, 2006; Baturin, 2011; Tribovillard et al., 2012; Westermann et al., 2013; Huo et al., 2022). When the slope of the average trend line in the Mo-TOC graph decreases, it indicates an increase in the degree of water restriction. This indicates that in a strongly restricted basin, the water is renewed slowly and Mo in the basin seawater is depleted, resulting in relatively low Mo enrichment in the sediment. The Mo/TOC values of the research samples range from 0.919 to 22.169, with an average of 5.569 and a trend line slope of 1.914. However, due to the R^2 value being only 0.221, it is considered that the reliability of this indicator is insufficient, and it is not possible to discuss the limitations of the water (Figure 9). We believe that the unreliability of this analysis may be related to the low abundance of organic matter and Mo concentration, making it highly susceptible to external factors.

Some scattered Mo_{EF} and U_{EF} points in the lower right were far from the open sea in a strongly restricted area. This indicated that the argillaceous limestone of $T_2l_3^2$ was deposited in a basin that was not strongly restricted (Algeo and Tribovillard, 2009) and that deposition occurred under suboxic-anoxic conditions (Figure 10). The overall characteristics of Mo/U were approximately equal to (0.1–3) × $(Mo/U)_{SW}$, and mainly distributed in (0.1–1) × $(Mo/U)_{SW}$. As the enrichment factor increases, the Mo_{EF}/U_{EF} ratio continues to increase, and the supply of Mo is not limited, which differs from the CT region (Huo et al., 2022). This indicates that although also in a semi-restricted environment, the seawater activity in the PY3 area is slightly stronger than that in the CT area.

5.5 Depositional model

Argillaceous limestone of $T_2l_3^2$ was also in a semi-restricted lagoon environment during the sedimentary period, with the eastern part restricted by the Luzhou and Kaijiang paleo-uplifts, and the western part slightly restricted by the dolomite tidal flat.

Based on the analysis of the above indicators, we believe that the decoupling between the development and preservation conditions of organic matter is an important factor in the depletion of organic matter in this argillaceous limestone in PY area. And this phenomenon is reflected in paragraphs I-III. In section I, lower salinity leads to insufficient algae development and stable low levels of paleoproductivity, resulting in insufficient organic matter production capacity in the ocean. Therefore, in this section, the *TOC* value can maintain a similar downward trend as the reducibility (Figures 2, 11a). In the lower part of section II, there was a sudden increase in salinity and paleoproductivity, and the level of algal development improved. However, due to the high oxidation of the water, organic matter enrichment remained difficult. A large amount of organic matter is rapidly decomposed during the sedimentation process. Nevertheless, due to the relative effect of paleoproductivity and redox conditions, the *TOC* value remained stable (Figures 2, 11b). When entering the upper part of section II, the reducibility was restored to some extent, but the salinity and paleoproductivity decreased to a certain extent, and the *TOC* value also decreased (Figures 2, 11c). In Stage III, the water undergoes severe oxidation, leading to a further decrease in organic matter content (Figures 2, 11d). It can be seen that throughout the

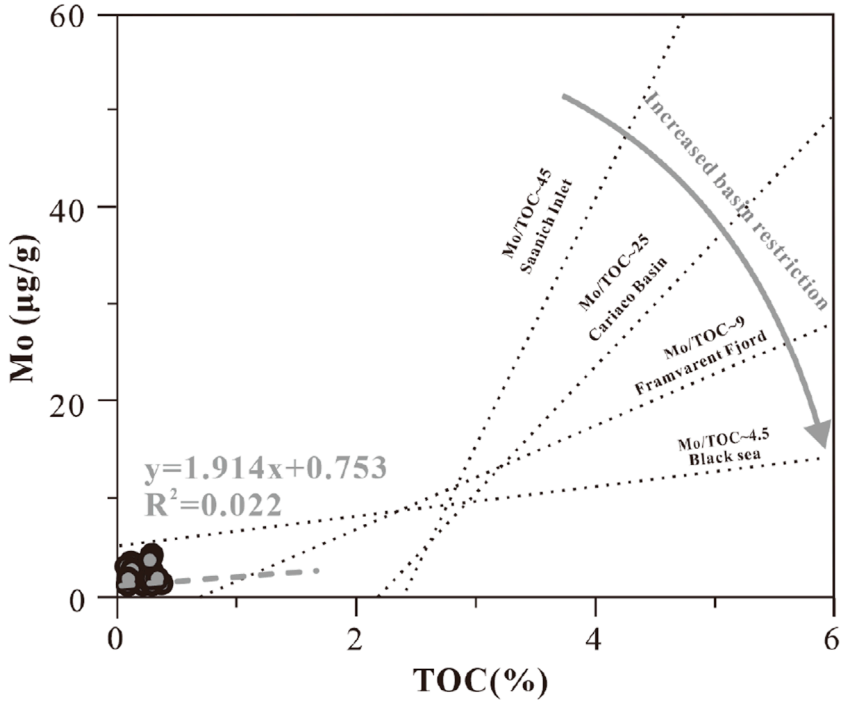

FIGURE 9
Mo-TOC model of argillaceous limestone in $T_2l_3^2$ in PY3 well.

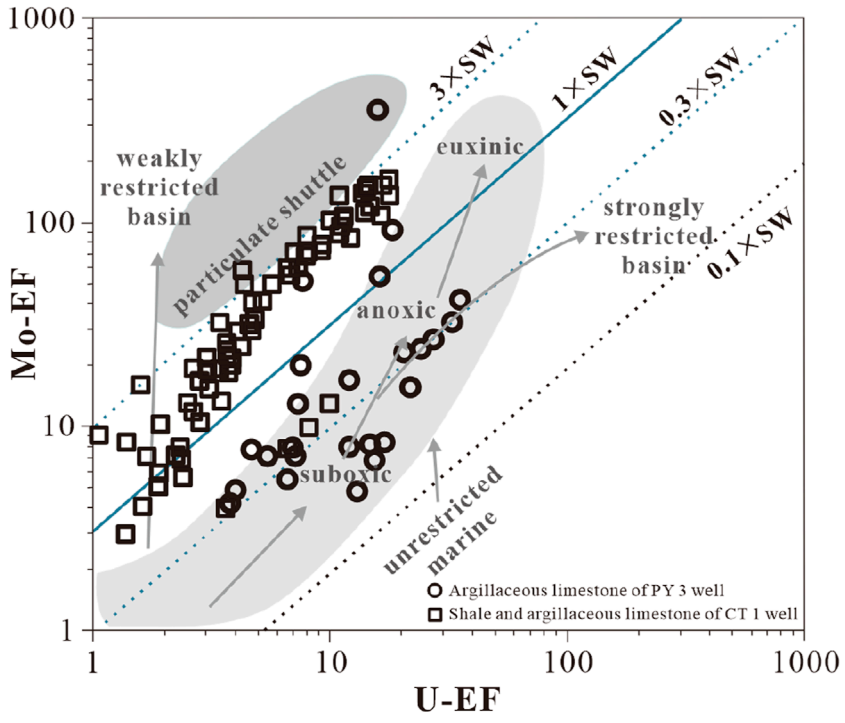

FIGURE 10
Mo_{EF}-U_{EF} model of argillaceous limestone in$T_2l_3^2$ (data of CT1 well according to Huo et al., 2022).

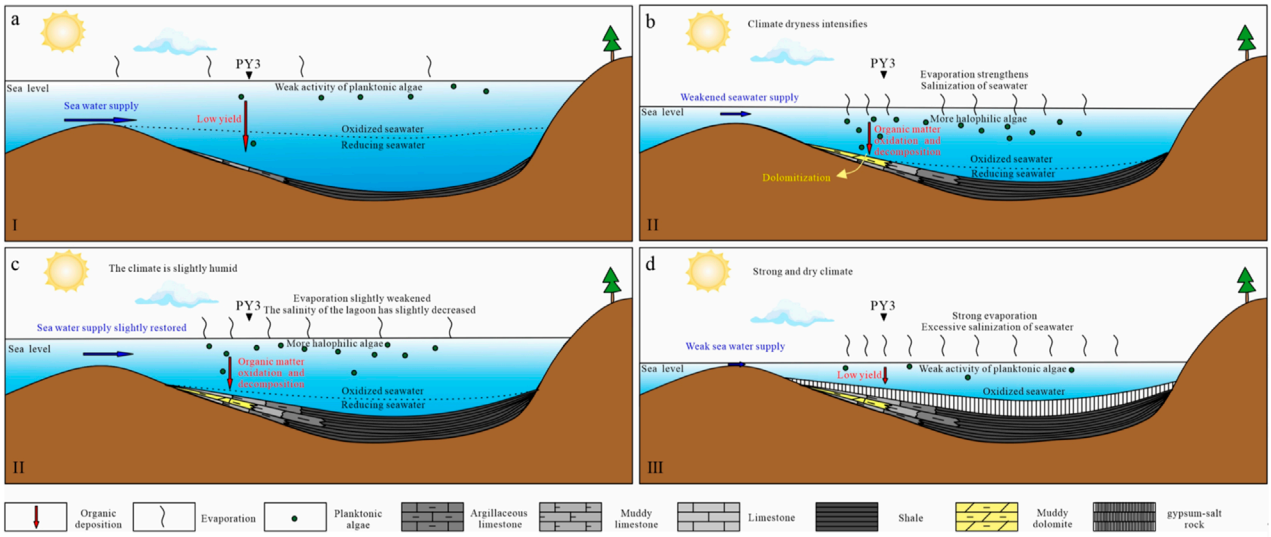

FIGURE 11
Salt controlled organic matter depletion model of argillaceous limestone in $T_2l_3^2$. **(a)** Stage of the I sedimentation; **(b)** Early stage of the II sedimentation; **(c)** Later stage of the II sedimentation; **(d)** Stage of the III sedimentation.

TABLE 3 Source rocks in high salinity water in East Asia.

System	Stratum	Country	Region	Environment	Lithology	*TOC* (%)	References
Triassic	Leikoupo Fm	China	Sichuan Basin	Gypsum-limy lagoon (edge)	Argillaceous limestone	0.11~0.34 (average: 0.21)	This study
Triassic	Leikoupo Fm	China	Sichuan Basin	Gypsum-limy lagoon	Calcareous shale	0.11~4.0 (average: 0.88)	Zhang et al. (2023)
Ordovician	Majiagou Fm	China	Ordos Basin	Gypsum lagoon	Dolomitic mudstone	0.30~8.45 (average: 1.14)	Tu et al. (2016)
Cambrian	Xishanbulake-Xidashan Fm	China	Tarim Basin	Shelf and restricted platform	Siliceous shale and calcareous shale	0.44~10.21 (average: 2.11)	Guo et al. (2023)
Paleogene	4th member of Shahejie Fm	China	Bohai Bay Basin	Salt lake	Mudstone	0.66~13.04 (average: 3.43)	Duan et al. (2022)
Permian	Fengcheng Fm	China	Junggar Basin	Salt lake	Mudstone	0.29~2.49 (average: 1.12)	Bai et al. (2024)

entire sedimentary period, paleoproductivity and redox conditions remained decoupled.

Based on existing petrological and geochemical evidence, this decoupling is mainly due to the mismatch between salinity and reducibility fluctuations caused by changes in sea level and seawater recharge (Figure 11). In the lagoon environment where limitations have increased and the climate has shifted from humid to semi humid, salinity has promoted the growth of some algae within suitable ranges. This process is accompanied by a decrease in sea level, an increase in dissolved oxygen in the water, and an improvement in productivity. However, the weakening of reduction conditions may promote the decomposition of organic matter by various bacteria, resulting in constraints on the preservation conditions of organic matter.

5.6 Further prospects

5.6.1 Importance of source rocks in high salinity environments

From a global perspective, the development of source rocks in high salinity lagoon facies is rare but meaningful (Huo et al., 2022). Multiple mechanism rich source rocks have been discovered in high salinity water in East Asia (Tu et al., 2016; Duan et al., 2022; Guo et al., 2023; Zhang et al., 2023; Bai et al., 2024; Table 3; Figure 12). Although high salinity may lead to organic matter mineralization, increasing discoveries may indicate a potential connection between the formation of source rocks in high salinity environments and life activities induced by water salinity. For example, the evolution of algae during changes in water salinity.

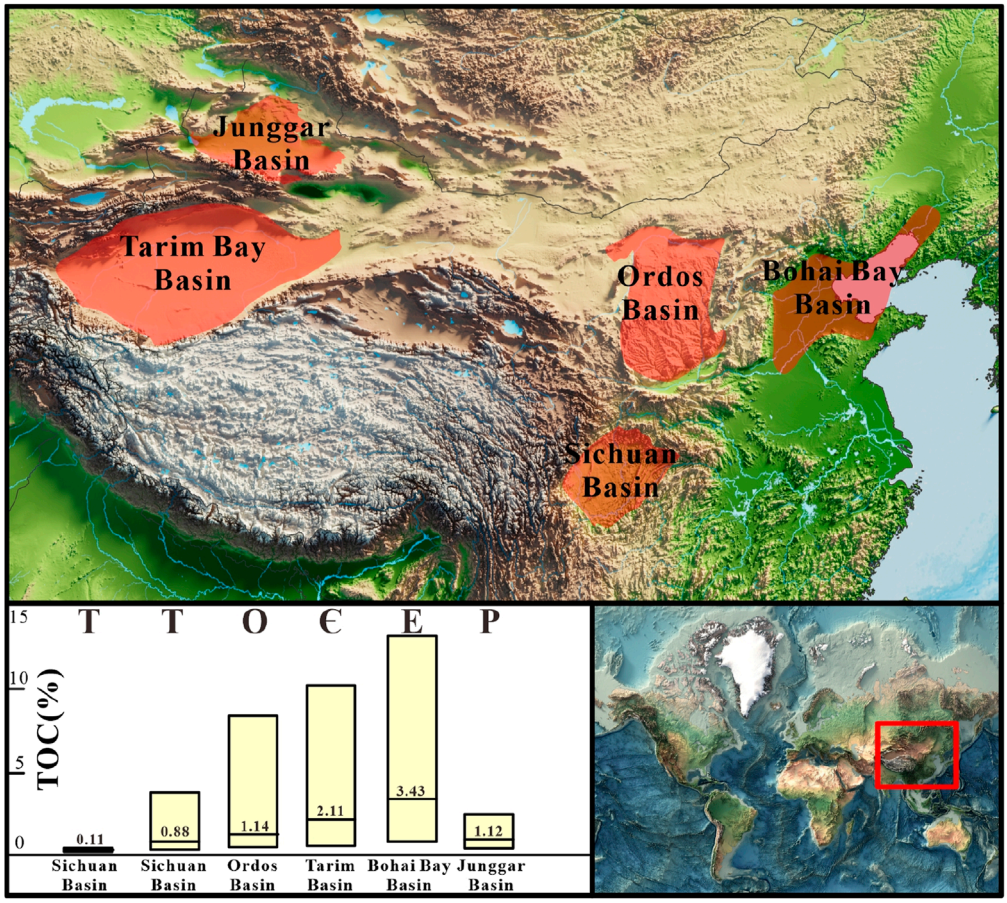

FIGURE 12
Distribution of source rocks deposited in high salinity environments in East Asia (TOC data from Tu et al., 2016; Duan et al., 2022; Guo et al., 2023; Zhang et al., 2023; Bai et al., 2024).

Furthermore, the development of source rocks in high salinity water provides new ideas for oil and gas exploration.

5.6.2 Shortcomings and potential of methods

In this study, a specific method was mainly provided: using biomarker compound indicators to reflect the degree of algal development, analyzing the correlation between paleosalinity indicators and algal development. To clarify the tolerance or preference of planktonic algae to salinity, and to using *TOC* values, paleoproductivity indicators, and algal development for correlation analysis to discuss their contribution to organic matter enrichment. However, it should be noted that in the application process, various potential influencing factors need to be considered and eliminated to ensure the reliability of the data.

Due to the recent discovery of calcareous shale and argillaceous limestone gas reservoirs in $T_2l_3^2$ of the Sichuan Basin, research materials are scarce. Therefore, the author only discussed the differences in organic matter enrichment in this semi-restricted lagoon facies formation through existing research materials, mainly to provide new research ideas. At present, there are still some relevant issues that need to be addressed, such as applying this method to multiphase zones and multi regional comparisons of contemporaneous strata to trace the migration patterns of algae producers during this period, or conducting quantitative analysis through more sophisticated means. With the further advancement of exploration and development, we hope to have more research materials in the future to provide further improvement for this method.

However, these phenomena still provide us with some ideas for searching for self-generated and self-stored carbonate rocks: (1) high salinity environments have the potential to promote organic matter production and form gypsum cap rocks to assist in *in-situ* oil and gas accumulation; (2) Although halophilic algae have poor environmental tolerance, they can rapidly develop in suitable environments. This characteristic seems to be able to explain the rapid and sudden development of large sets of source rocks in high salinity environments. This study and the potential issues arising from it respond to the relationship between ecological recovery and organic matter enrichment. At the same time, providing a possible model for the formation of "source-reservoir-cap" rock combinations formed by organic rich carbonate rocks and evaporite.

6 Conclusion

(1) The lithology of $T_2l_3^2$ in the PY area of the Sichuan Basin is mainly composed of argillaceous limestone, with the main reservoir spaces being clay intergranular pores and organic matter pores.

(2) The kerogen type of argillaceous limestone of $T_2l_3^2$ is I-II_1, and the organic matter mainly comes from halophilic algae in reducing seawater, mixed with a very small amount of terrestrial organic matter. Compared to the source rock of $T_2l_3^2$ inCT1 well, its organic matter abundance is low and the hydrocarbon generation capacity is weak.

(3) The organic matter enrichment of argillaceous limestone of $T_2l_3^2$ in the PY area of the Sichuan Basin is controlled by a combination of redox conditions, paleosalinity, and paleoproductivity. The ancient salinity mainly induces the development of halophilic algae, promotes the improvement of primary productivity, and provides conditions for organic matter production. The reducibility of water provides conditions for the preservation of organic matter. The decoupling of organic matter development and preservation conditions is the main cause of organic matter depletion in the research subjects.

Data availability statement

The original contributions presented in the study are included in the article/supplementary material, further inquiries can be directed to the corresponding author.

Author contributions

YH: Conceptualization, Data curation, Formal Analysis, Investigation, Methodology, Software, Visualization, Writing – original draft. YW: Conceptualization, Data curation, Formal Analysis, Methodology, Project administration, Writing – review and editing. HW: Funding acquisition, Methodology, Project administration, Supervision, Writing – review and editing. FH: Investigation, Methodology, Software, Supervision, Writing – review and editing. XW: Investigation, Software, Visualization, Writing – review and editing. RG: Investigation, Software, Visualization, Writing – review and editing. YL: Investigation, Visualization, Writing – review and editing. YR: Conceptualization, Investigation, Methodology, Writing – review and editing. HJ: Investigation, Methodology, Writing – review and editing.

Funding

The author(s) declare that financial support was received for the research and/or publication of this article. The authors would like to acknowledge financial support provided by Sichuan Provincial Youth Science and Technology Innovative Research Group Fund (No. 2022JDTD0004).

Acknowledgments

We would like to thank Professor Huaguo Wen of Chengdu University of Technology for his support.

Conflict of interest

The authors declare that the research was conducted in the absence of any commercial or financial relationships that could be construed as a potential conflict of interest.

Generative AI statement

The authors declare that no Generative AI was used in the creation of this manuscript.

Publisher's note

References

Adams, J. A. S., and Weaver, C. E. (1958). Thorium-to-uranium ratios as indicators of sedimentary processes; example of concept of geochemical facies. *American. Association of Petroleum Geologist Bulletin* 42, 387–430

Ahmad, F., Baioumy, H., Farouk, S., Al-Kahtany, K., El-Sorogy, A., and Kirk, J. (2019). Geochemistry and stable isotopes of the upper campanian–lower maastrichtian phosphorite-bearing sequence, Central Jordan: implications for their age, origin, and diagenesis. *Geol. J.* 55, 4453–4468. doi:10.1002/gj.3692

Algeo, T. J., and Lyons, T. W. (2006). Mo—total organic carbon covariation in modern anoxic marine environments: implications for analysis of paleoredox and paleohydrographic conditions. *Paleoceanography* 21 (1), 279–298. doi:10.1029/2004pa001112

Algeo, T. J., and Tribovillard, N. (2009). Environmental analysis of paleoceanographic systems based on molybdenum–uranium covariation. *Chem. Geol.* 268 (3-4), 211–225. doi:10.1016/j.chemgeo.2009.09.001

Aplin, A. C., and Macquaker, J. H. S. (2011). Mudstone diversity: origin and implications for source, seal, and reservoir properties in petroleum systems. *AAPG Bull.* 95 (12), 2031–2059. doi:10.1306/03281110162

Bai, Y. B., Li, M. Y., Zhu, T., Zhao, J. Z., Ren, H. J., Wu, W. T., et al. (2024). Geochemical characteristics of source rocks and sweet spot evaluation of shale oil in Permian Fengcheng Formation in Mahu Sag. *Lithol. Reserv.* 36 (06), 110–121.

Baturin, G. N. (2011). Geochemistry of sapropel in the black sea. *Geochem. Int.* 49 (5), 531–535. doi:10.1134/s0016702911050028

Bottjer, D. J., Clapham, M. E., Fraiser, M. L., and Powers, C. M. (2008). Understanding mechanisms for the end-Permian mass extinction and the protracted Early Triassic aftermath and recovery. *GSA Today* 18, 4–10. doi:10.1130/gsatg8a.1

Brand, U., and Veizer, J. (1981). Chemical diagenesis of a multicomponent carbonate system; 2, Stable isotopes. *J. Sediment. Res.* 51 (3), 987–997.

Calvert, S. E., and Pedersen, T. F. (1993). Geochemistry of Recent oxic and anoxic marine sediments: implications for the geological record. *Marine Geology.* 113 (1-2), 67–88. doi:10.1016/0025-3227(93)90150-T

Canfield, D. E. (1994). Factors influencing organic carbon preservation in marine sediments. *Chem. Geol.* 114 (3-4), 315–329. doi:10.1016/0009-2541(94)90061-2

Cao, Q. Y. (1985). Identifcation of microcomponents and types of kerogens under transmitted light J1. *Petroleum Explor. Dev.* 6 (5), 14–24.

Chen, L., Jin, A. A., Ma, X. J., Wu, D., and Feng, H. J. (2022). Research progress on osmotic pressure adaptation strategy and salt tolerance enhancement of microorganisms under high salinity environment. *Acta Microbiol. Sin.* 62 (9), 3306–3317.

Chen, S. Y., Wang, S. M., and Shen, J. (2003). Variations of sedimentary environments during late Cenozoic of Co Ngoin,Central Tibetan plateau and its tectonic uplift implications. *J. Lake Sci.* 15 (1), 21–27. doi:10.18307/2003.0103

Chu, Y., Faure, M., Lin, W., Wang, Q. C., and Ji, W. B. (2012). Tectonics of the Middle Triassic intracontinental Xuefengshan Belt, South China: new insights from structural and chronological constraints on the basal décollement zone. *Int. J. Earth Sci.* 101, 2125–2150. doi:10.1007/s00531-012-0780-5

Dai, J. X. (1981). Geographical distribution of oil and gas discovered in ancient China. Oil and Gas Geology. *(3)* 292-299, 305.

Duan, W., Zeng, X., Cai, J. G., Li, Z., Wang, C. X., and Lin, R. (2022). The control of sedimentary environment and paleoproductivity on the formation of high-quality source rocks in Dongying Sag, Bohai Bay Basin-Taking the Shahejie Formation in Niuzhuang Subsag as an example. *Nat. Gas. Geosci.* 33 (11), 1754–1767.

Ernst, W. (1970). *Geochemical facies analysis*. Amsterdam: Elsevier.

Farouk, S., Nagy, J., El-Dawoudi, I. A., Ahmad, F., and Al-Kahtany, K. (2024a). Response of Bathonian-Oxfordian transgressive-regressive cycles on foraminiferal morphogroups, and diversity: a case study from shallow marine deposits in north Gulf of Suez, Egypt. *Lethaia* 57 (3), 1–16. doi:10.18261/let.57.3.6

Farouk, S., Sen, S., Abu-Alam, T., Al-Kahtany, K., and Abioui, M. (2022). Geomechanical assessment of the lower turonian AR-F limestone member, abu gharadig field, Egypt: implications for unconventional resource development. *Front. Earth Sci.* 10. doi:10.3389/feart.2022.1041453

Farouk, S., Sen, S., Ahmed, F., Qteishat, A., Al-Kahtany, K., Moreno, H. M., et al. (2024b). Assessment of the upper cretaceous abu roash carbonate source rocks from the beni suef field, western desert, Egypt. *J. Afr. Earth Sci.* 215, 105272. doi:10.1016/j.jafrearsci.2024.105272

Farouk, S., Sen, S., Ganguli, S. S., Ahmed, F., Abioui, M., Al-Kahtany, K., et al. (2023). An integrated petrographical, petrophysical and organic geochemical characterization of the Lower Turonian Abu Roash-F carbonates, Abu Gharadig field, Egypt – inferences on self-sourced unconventional reservoir potential. *Mar. Petroleum Geol.* 145, 105885. doi:10.1016/j.marpetgeo.2022.105885

Fedo, C. M., Wayne Nesbitt, H., and Young, G. M. (1995). Unraveling the effects of potassium metasomatism in sedimentary rocks and paleosols, with implications for paleoweathering conditions and provenance. *Geology* 23 (10), 921–924. doi:10.1130/0091-7613(1995)023<0921:uteopm>2.3.co;2

Feng, Z. Z., Li, S. W., Yang, Y. Q., and Jin, Z. K. (1997). Potential of oil and gas of the Permian of south China from the viewpoint of lithofacies paleogeography. *Acta Pet. Sin.* 18 (1), 10–17.

Floyd, P. A., Keele, B. E., Leveridge, B. E., Franke, W., Shail, R., and Dörr, W. (1990). Provenance and depositional environment of rhenohercynian synorogenic greywackes from the Giessen Nappe, Germany. *Geol. Rundsch.* 79 (3), 611–626. doi:10.1007/bf01879205

Guo, T. T., Zhu, B., Yang, T., and Chen, Y. Q. (2023). Sedimentary environment evolution of lower cambrian xishanbulake-xidashan Formation in tarim basin. *Pet. Exp. Geol.* 45 (02), 252–265.

Hatch, J. R., and Leventhal, J. S. (1992). Relationship between inferred redox potential of the depositional environment and geochemistry of the Upper Pennsylvanian (Missourian) stark shale member of the Dennis Limestone, Wabaunsee county, Kansas, United States. *Chem. Geol.* 99 (1-3), 65–82. doi:10.1016/0009-2541(92)90031-y

He, D. F., Ma, Y. S., Cai, X. Y., Zhang, J., and Zhang, Y. J. (2017). Comparison study on controls of geologic structural framework upon hydrocarbon distribution of marine basins in western China. *Acta Petrol. Sin.* 33 (4), 1037–1057.

He, J., Zhang, S., Zhang, X., He, H., and Wu, H. (2016). Composition and distribution characteristicsand geochemical significance of n-alkanes in core sediments in the northern part of the south Yellow Sea. *J. Chem.* 2016 (1), 1–9. doi:10.1155/2016/4741939

He, L. J., Xu, H. H., and Wang, J. Y. (2011). Thermal evolution and dynamic mechanism of the Sichuan Basin during the early permian-Middle Triassic. *Sci. China Earth Sci.* 54, 1948–1954. doi:10.1007/s11430-011-4240-z

Huang, H. Y., He, D. F., Li, Y. Q., and Fan, H. D. (2019). Determination and formation mechanism of the luzhou paleo-uplift in the southeastern Sichuan Basin. *Earth Sci. Front.* 26 (1), 102–120.

Huang, J. Z. (1998). Classification basis of stable carbon isotope of kerogen. *Geol. Geochem.* 16 (3), 66–68.

Huo, F., Wen, H. G., Li, L., Luo, B., Zhou, G., Xu, W. L., et al. (2022). Influence of the depositional environment on the formation of organic-rich marine shale: a case study of the first discovery of anisian shale in the Sichuan Basin. *J. Petroleum Sci. Eng.* 214, 110577. doi:10.1016/j.petrol.2022.110577

Katz, B. J., Dittmar, E. I., and Ehret, G. E. (2008). A geochemical review of carbonate source rocks in italy. *Journal of Petroleum Geology* 23 (4), 399–424. doi:10.1111/j.1747-5457.2000.tb00494.x

Li, Q., Shi, J. B., and Xin, Y. G. (2025). Hydrocarbon accumulation conditions and exploration direction of argillaceous-dolomite unconventional gas reservoirs in the 2nd sub-member of the first member of Leikoupo Formation in Hechuan-Tongnan area of Sichuan Basin. *Petroleum Geol. and Oilfield Dev. Daqing.*

Li, Y. Q., He, S. J., Gao, D. F., Gao, J., Wang, Y. C., Huang, H. Y., et al. (2021). Middle Triassic tectono-sedimentary development of Sichuan Basin: Insights into the cratonic differentiation. *Geol. J.* 56 (4), 1858–1878. doi:10.1002/gj.4033

Makky, A. F., El Sayed, M. I., El-Ata, A. S. A., Abd El-Gaied, I. M., Abdel-Fattah, M. I., and Abd-Allah, Z. M. (2014). Source rock evaluation of some upper and lower cretaceous sequences, West Beni Suef concession, Western Desert, Egypt. *Egypt. J. Petroleum* 23 (1), 135–149. doi:10.1016/j.ejpe.2014.02.016

Maloof, A. C., Porter, S. M., Moore, J. L., Dudás, F. Ö., Boweing, S. A., Higgins, J. A., et al. (2010). The earliest Cambrian record of animals and ocean geochemical change. *GSA Bulletin* 122 (11-12), 1731–1774. doi:10.1130/B30346.1

Marynowski, L., Narkiewicz, M., and Grelowski, C. (2000). Biomarkers as environmental indicators in a carbonate complex, example from the middle to upper Devonian, Holy Cross Mountains, Poland. *Sediment. Geol.* 137 (3-4), 187–212. doi:10.1016/s0037-0738(00)00157-3

McLennan, S. M. (1993). Weathering and global denudation. *J. Geol.* 101 (2), 295–303. doi:10.1086/648222

Meng, Q. R., Wang, E., and Hu, J. M. (2005). Mesozoic sedimentary evolution of the northwest Sichuan Basin: Implication for continued clockwise rotation of the South China block. *Geol. Soc. Am. Bull.* 117 (3), 396–410. doi:10.1130/b25407.1

Miao, J. J., Wu, X. Q., Song, X. B., Zheng, L. J., Chen, Y. B., and Zeng, H. S. (2022). Effectiveness of marine carbonate source rocks: a case study of Middle Triassic Leikoupo Formation in Western Sichuan Depression. *Petroleum Geol. Exp.* 44 (2), 241–250.

Murray, R. W. (1994). Chemical criteria to identify the depositional environment of chert: general principles and applications. *Sedimentary Geology.* 90 (3-4), 213–232. doi:10.1016/0037-0738(94)90039-6

Nance, W. B., and Taylor, S. R. (1976). Rare earth element patterns and crustal evolution—i. Australian post-archean sedimentary rocks. *Geochimica Cosmochimica Acta* 40 (12), 1539–1551. doi:10.1016/0016-7037(76)90093-4

Nesbitt, H. W., and Young, G. M. (1982). Early Proterozoic climates and plate motions inferred from major element chemistry of lutites. *nature* 299 (5885), 715–717. doi:10.1038/299715a0

Nie, H. K., Zhang, G. R., Li, P., Ding, J. H., Dang, W., Sun, C. X., et al. (2022). Resrarch status and prospect on organic matter pores in shale. *Acta Pet. Sin.* 43 (12), 1770–1787.

Panahi, A., Young, G. M., and Rainbird, R. H. (2000). Behavior of major and trace elements (including REE) during Paleoproterozoic pedogenesis and diagenetic alteration of an Archean granite near Ville Marie, Québec, Canada. *Geochimica Cosmochimica Acta* 64 (13), 2199–2220. doi:10.1016/s0016-7037(99)00420-2

Philippi, G. T. (1974). The influence of marine and terrestrial source material on the composition of petroleum.*Geochimica Cosmochimica Acta* 38 (6), 947–966. doi:10.1016/0016-7037(74)90067-2

Qiu, X., Liu, C., Wang, F., Deng, Y., and Mao, G. (2015). Trace and rare earth element geochemistry of the Upper Triassic mudstones in the southern Ordos Basin, Central China. *Cent. China. Geol. J.* 50 (4), 399–413. doi:10.1002/gj.2542

Qteishat, A., El-Shafeiy, M., Farouk, S., Ahmad, F., Al-Kahtany, K., Gentzis, T., et al. (2024). Organic geochemical characterization and hydrocarbon generation modeling of paleozoic-paleogene shales, Wadi Sirhan basin, south-eastern Jordan. *Mar. Petroleum Geol.* 170, 107152. doi:10.1016/j.marpetgeo.2024.107152

Ruan, Y. B., Zhou, G., Huo, F., Sun, H. F., Guo, P., Luo, T., et al. (2022). Source-reservoir characteristics and configuration of the third member of Middle Triassic Leikoupo Formation in central Sichuan Basin. *Lithol. Reserv.* 34 (5), 139–151.

Sageman, B., Meyers, S. R., and Lyons, T. W. (2003). Role of sulfate reduction in organic matter degradation and molybdenum accumulation: Theoretical framework and application to Cenomanian-Turonian organic matter burial event. *Geochmica et Cosmochimica Acta*.

Sahoo, A. K., Basu, S., Vishal, V., and Srivastava, M. (2020). Hierarchical clustering of pristane and phytane data to identify the sweet spots in the shale reservoirs. *Energy Clim. Change* 1, 100011. doi:10.1016/j.egycc.2020.100011

Sun, H. F., Luo, B., Wen, L., Wang, J. X., Zhou, G., Wen, H. G., et al. (2021). The first discovery of organic-rich shale in Leikoupo Formation and new areas of subsalt exploration, Sichuan Basin. *Nat. Gas. Geosci.* 32 (2), 233–247.

Tan, X. C., Li, L., Liu, H., Cao, J., Wu, X. Q., Zhou, S. Y., et al. (2014). Mega-shoaling in carbonate platform of the Middle Triassic Leikoupo Formation, Sichuan Basin, southwest China. *Sci. China Earth Sci.* 57 (03), 465–479. doi:10.1007/s11430-013-4667-5

Tang, D. J., Shi, X. Y., Zhao, X. K., Wang, X. Q., and Song, G. Y. (2015). Mo-U covariation as an important proxy for sedimentary environment redox conditions - progress, problems and prospects. *Geosciences* 29 (1), 1–13.

Tribovillard, N., Algeo, T. J., Lyons, T., and Riboulleau, A. (2006). Trace metals as paleoredox and paleoproductivity proxies: an update. *Chemical Geology* 232 (1-2), 12–32. doi:10.1016/j.chemgeo.2006.02.012

Tribovillard, N., Algeo, T. J., Baudin, F., and Riboulleau, A. (2012). Analysis of marine environmental conditions based onmolybdenum–uranium covariation—applications to mesozoic paleoceanography. *J. Chem. Geol.* 324: 46–58.

Tu, J. Q., Dong, Y. G., Zhang, B., Nan, H. L., Li, C. J., Wang, X. M., et al. (2016). The discovery of large-scale effective source rocks in the Ordovician Majiagou Formation in the Ordos Basin and its geological significance. *Nat. Gas. Ind.* 36 (05), 15–24.

Ungerer, P. (1990). State of the art of research in kinetic modelling of oil formation and expulsion. *Org. Geochem.* 16 (1-3), 1–25. doi:10.1016/0146-6380(90)90022-r

Uratani, J. M., Kumaraswamy, R., and Rodríguez, J. (2014). A systematic strain selection approach for halotolerant and halophilic bioprocess development: a review. *Extremophiles* 18 (4), 629–639. doi:10.1007/s00792-014-0659-4

Wang, C. Y. (2018). *Research on molecular mechanism of polycylic aromatic hydrocarbons degradation by halophiles*. Beijing: Tsinghua University.

Wang, H., Liu, S. G., Qin, C., Zhang, C. J., Wang, G. Z., Li, D. X., et al. (2009). Study on petroleum geological conditions and hydrocarbon exploration direction of Leikoupo Formation in the centre and west of Sichuan Basin China. *J. Chengdu Univ. Technol. Sci. Technol. Ed.* 36 (6), 669–674.

Wang, Y. J., Fan, W. M., Zhang, G. W., and Zhang, Y. H. (2013). Phanerozoic tectonics of the South China Block: Key observations and controversies. *Gondwana Res.* 23 (4), 1273–1305. doi:10.1016/j.gr.2012.02.019

Wang, Z. C., Xin, Y. G., Xie, W. R., Wen, L., Zhang, H., Xie, Z. Y., et al. (2023). Petroleum geology of marl in Triassic Leikoupo Formation and discovery significance of well chongtan1 in central Sichuan Basin, SW China. *Petroleum Explor. Dev.* 50 (5), 1092–1104. doi:10.1016/s1876-3804(23)60451-3

Wen, H. G., Huo, F., Guo, P., Ning, M., Liang, J. T., Zhong, Y. J., et al. (2021). Advances and prospects of dolostone-evaporite paragenesis system. *Acta Pet. Sin.* 39 (06), 1321–1343.

Westermann, S., Stein, M., Matera, V., Fiet, N., Fleitmann, D., Adatte, T., et al. (2013). Rapid changes in the redox conditions of the western tethys ocean during the early aptian oceanic anoxic event. *J. Geochimica Cosmochimica Acta* 121, 467–486. doi:10.1016/j.gca.2013.07.023

Wu, X. Q., Liu, Q. Y., Chen, Y. B., Zhai, C. B., Ni, C. H., and Yang, J. (2020). Constraints of molecular and stable isotopic compositions on the origin of natural gas from Middle Triassic reservoirs in the chuanxi large gas field, Sichuan Basin, SW China. *J. Asian Earth Sci.* 204, 104589. doi:10.1016/j.jseaes.2020.104589

Xiao, H., Li, M. J., Wang, T. G., and Leng, J. Y. (2022). Typical molecular marker assemblage of the mesoproterozoic sediments: a case study of the xiamaling Formation black shales in the xuanlong depression. *Acta Sedimentol. Sin.* 40 (2), 547–556.

Xin, Y. G., Zhou, J. G., Ni, C., Gu, M. F., Gong, Q. S., Dong, Y., et al. (2013). Sedimentary facies features and favorable lithofacies distribution of Middle Triassic Leikoupo barriered carbonate platform in Sichuan Basin. *Mar. Orig. Pet. Geol.* 18 (2), 1–7.

Yang, C. (2017). *The developmental characteristics and controlling factors of organic associated pores in organic rich shales*. Beijing: China University of Geosciences.

Zeman-Kuhnert, S., Heim, C., Oeztoprak, M., and Thiel, V. (2023). Reconstructing eutrophication trends of a shallow lake environment using biomarker dynamics and sedimentary sterols. *Org. Geochem.* 177, 104555. doi:10.1016/j.orggeochem.2023.104555

Zeng, D. M., Wang, X. Z., Zhang, F. S., Zhang, Q., Zhang, R. X., Zhu, Y. G., et al. (2007). Study on reservoir of the Leikoupo Formation of Middle Triassic in northwestern Sichuan Basin. *J. Palaeogeogr. Chin. Ed.* 9 (3), 253–266.

Zhang, B. J., Sun, H. F., Luo, Q., Zeng, H. C., Xu, L., Li, L., et al. (2023). Geochemical characteristics and hydrocarbon origin of Leikoupo Formation platform lagoon facies shale in central Sichuan Basin. *Nat. Gas. Ind.* 43 (6), 15–29.